

Constraints on the equation-of-state from low energy heavy-ion collisions within the PHQMD microscopic approach with momentum-dependent potential

Viktar Kireyeu¹, Vadim Voronyuk¹, Michael Winn² Susanne Gläsel³, Jörg Aichelin^{2,4},
Christoph Blume^{3,5,6}, Elena Bratkovskaya^{5,6,7}, Gabriele Coci⁸, Jiaying Zhao^{6,7}

¹ *Joint Institute for Nuclear Research, Joliot-Curie 6, 141980 Dubna, Moscow region, Russia*

² *SUBATECH, Nantes University, IMT Atlantique,*

IN2P3/CNRS 4 rue Alfred Kastler, 44307 Nantes cedex 3, France

³ *Institut für Kernphysik, Max-von-Laue-Str. 1, 60438 Frankfurt, Germany*

⁴ *Frankfurt Institute for Advanced Studies, Ruth Moufang Str. 1, 60438 Frankfurt, Germany*

⁵ *GSI Helmholtzzentrum für Schwerionenforschung GmbH, Planckstr. 1, 64291 Darmstadt, Germany*

⁶ *Helmholtz Research Academy Hessen for FAIR (HFHF),*

GSI Helmholtz Center for Heavy Ion Physics. Campus Frankfurt, 60438 Frankfurt, Germany

⁷ *Institut für Theoretische Physik, Johann Wolfgang Goethe University,*

Max-von-Laue-Str. 1, 60438 Frankfurt, Germany and

⁸ *Dipartimento di Fisica e Astronomia “E. Majorana”,*

Università degli Studi di Catania, Via S. Sofia, 64, I-95125 Catania, Italy

(Dated: November 8, 2024)

We investigate the influence of the equation-of-state (EoS) of nuclear matter on collective observables, the directed (v_1) and the elliptic flow (v_2) of nucleons and light clusters in heavy-ion collisions at GeV beam energies employing the Parton-Hadron-Quantum-Molecular Dynamics (PHQMD) microscopic transport approach. Here the clusters are formed dynamically during the entire heavy-ion collision by potential interaction between nucleons, including additionally deuteron production by hadronic kinetic reactions. We employ three different EoS - realized via potential interactions: two static EoS, dubbed 'soft' and 'hard', which differ in the compressibility modulus, as well as a soft momentum dependent EoS, adjusted to pA elastic scattering data. We find that the momentum dependent potential has different consequences for rapidity and transverse momentum spectra than for flow coefficients. We obtain the best description of the HADES and FOPI data on the directed and elliptic flow coefficients of protons and light clusters applying a momentum dependent EoS. Moreover, we observe a scaling behavior of v_2 versus p_T with atomic number A . Finally we demonstrate that flow observables can help to identify the cluster production mechanisms.

I. INTRODUCTION

The exploration of the nuclear equation-of-state (EoS) is one of the major objectives in nuclear physics. Experimentally its study started with the first heavy-ion experiments at the Bevalac accelerator in Berkeley [1], where for the first time nuclear densities well above normal nuclear matter density could be obtained in the laboratory. Later also complimentary information has been obtained from the observed mass-radius relations of neutron stars [2–5] and even more recently first attempts have been made to obtain information about the nuclear equation-of-state from gravitational waves [6, 7].

At densities well above normal nuclear matter density, ρ_0 , the EoS cannot be determined by nuclear matter calculations because there the expansion schemes of the Brückner G-matrix [8], as well as of the chiral perturbation approach, break down [9]. Therefore, the theoretical interpretation of heavy-ion experiments is the only way to study the EoS systematically. In these experiments the EoS is, however, not directly measured and consequently it is a challenge for theory to identify those experimental observables which are sensitive to the EoS and to predict them with sufficient precision that a comparison with experimental results is meaningful. It turned out that at beam energies around 1 GeV/nucleon, where, on the one side, densities up to three times nuclear matter density

can be reached and, on the other side, meson production is not very frequent, the nucleon dynamics is very sensitive to the potential interaction, which is directly related to the EoS of nuclear matter [9–20]. These studies revealed that - besides subthreshold kaon production - the directed and elliptic flow are among the the most promising experimental signals which can be used for the determination of the EoS.

The theoretical prediction within microscopic transport approaches is challenging since flow coefficients are very sensitive not only to the employed potentials, which reflect the equation-of-state, but also to the properties of hadrons in the medium and their collisions. They depend also strongly on the centrality of the reaction what makes a detailed comparison with experiments complicated. In addition, the signals are that tiny that different numerical realizations of the transport approaches start to play a role.

To determine the EoS by analyzing the experimental results with the help of transport approaches is therefore a complicated task. In earlier transport calculations the EoS had been considered as static and from the first Plastic Ball data [1] it has been concluded that the nuclear EoS is rather hard [21]. Later one realized that the momentum-dependence of the nuclear interaction [22] has a strong influence on the flow observables [10, 11]. Static and momentum-dependent interactions,

which yield the same EoS for cold matter, influence the observables in heavy-ion reactions in a quite different way - cf. the reviews [23–25]. The momentum dependence of the nucleon-nucleon potential plays therefore a crucial role when heavy-ions collide with a beam energy in the GeV region [11, 15, 16, 26, 27]. Earlier calculations, which include these momentum-dependent interactions, point towards a soft momentum-dependent potential between baryons.

In the meantime the transport approaches have been advanced and, even more important, several data sets for Au+Au collisions at very similar energies from the HADES and FOPI collaborations became available. In these experiments also the directed v_1 and elliptic v_2 flow of light clusters has been measured, which allows for the first time to extend the EoS studies to light clusters. This is possible despite of the fact that the origin of cluster production at midrapidity is still debated. Even more, the study of the flow of light clusters may help to identify the way they are produced, as we will show in this article.

Light clusters at midrapidity have been found in heavy-ion experiments from beam energies of a couple of hundred MeV per nucleon up to the highest presently available energies of $\sqrt{s}=5.02$ TeV [28–32]. The slope of the transverse momentum spectra of all particles at midrapidity is almost independent of the beam energy and in the order of 100 MeV [33]. The excitation function of the multiplicity is rather smooth [31, 34]. Both observations point to an energy independent formation mechanism. One of the challenges for theory is how such clusters, weakly bound objects with a binding energy of the order of a couple of MeV (and in the case of hypertriton as low as about 130 keV), can survive in such an environment.

Several propositions have been advanced to understand the production of light clusters at midrapidity:

i) Clusters are formed according to phase space at a given temperature and a given chemical potential [35]. These statistical models assume implicitly that the clusters are formed in a thermal environment and that after creation they do not interact anymore. Statistical models are not able to make predictions on collective flow without additional assumptions.

ii) Clusters are formed by coalescence [36–41] assuming that after their last collision nucleons form clusters if the relative distance between the entrained nucleons in momentum and coordinate space is smaller than a given Δr_0 and Δp_0 .

iii) Clusters are formed by the same potential interaction [13, 42–44] which also determines the time evolution of the baryons in the semi-classical heavy-ion transport approaches.

iv) Deuterons are formed by three-body collisions like $NNN \rightarrow dN$ and $NN\pi \rightarrow d\pi$ and destroyed by the inverse reaction [44–46]. The cross sections for πd and Nd are known but the rate for the inverse reaction can only be obtained with additional approximations, which differ in different approaches. The collisional production of clusters is presently limited to deuterons.

Although there are observables which are sensitive to these cluster production mechanisms, the presently available data do not allow for an experimental distinction on the basis of the measured rapidity and p_T distribution of the clusters [47].

The goal of our study here is therefore twofold:

- to investigate the equation-of-state (EoS) of strongly interacting hadronic matter, created in heavy-ion collisions, by analyzing the directed flow v_1 and the elliptic flow v_2 of protons and light clusters.
- to investigate whether the collective flow observables v_1 and v_2 can distinguish between different theoretical models for cluster production in heavy-ion collisions.

For this purpose we calculate v_1 and v_2 of protons and different clusters as a function of rapidity y and transverse momentum p_T for different EoS and for different cluster production mechanisms employing Parton-Hadron-Quantum-Molecular Dynamics (PHQMD), a microscopic transport approach [41–44, 47]. In the PHQMD approach we have the possibility to compare the dynamical (potential + kinetic) and the coalescence production mechanisms directly, because both are applied to the same physical events and therefore the environment is identical. This allows to study directly the consequences of the different production mechanisms. We confronted our calculations with the experimental data from the HADES [48, 49] and FOPI Collaborations [50] at SIS energies. Also we relate our observations to recent results of UrQMD [26, 51] and SMASH [27].

Our paper is organized as follows: we start with the model description in Section II. In Section III we discuss the consequences of the different EoS for heavy-ion dynamics at SIS energies. Our results on flow coefficients in comparison to the HADES and FOPI data are presented in Section IV. The comparison of the flow of deuterons for different deuteron production mechanisms is discussed in Section V while our findings are summarized in Section VI. We will use the $\hbar = c = 1$ convention.

II. MODEL DESCRIPTION: PHQMD

The Parton-Hadron-Quantum-Molecular Dynamics (PHQMD) [41–44, 47] is a microscopic n-body transport model, which combines the characteristics of baryon propagation from the Quantum Molecular Dynamics (QMD) model [11, 13, 52, 53] and the dynamical properties and interactions in- and out-of-equilibrium of hadronic and partonic degrees-of-freedom of the Parton-Hadron-String-Dynamics (PHSD) approach [54–59]. We refer to these papers for the details and discuss here only the novelties and their consequences.

A. Momentum-dependent potential

In the previous PHQMD calculations we employed a static nucleon-nucleon interaction. In reality this interaction is momentum-dependent as can be seen by analysing the beam energy dependence of elastic pA scattering data [60, 61]. Usually these data are analyzed by comparing the data with solutions of the Dirac equation with scalar U_s and vector potentials with the zero component U_0 . These are displayed in ref.[60, 61]. To obtain a nucleon-nucleon potential, which we can employ in QMD type calculations, we have to calculate first the Schrödinger equivalent potential U_{SEQ} [62]

$$U_{SEQ}(p) = U_s + U_0 + \frac{2}{m_N}(U_s^2 - U_0^2) + \frac{U_0}{m} \sqrt{p^2 + m^2}, \quad (1)$$

where p is the momentum of the incoming proton in the target rest system. Our fit of this potential is displayed in Fig. 1 together with the points extracted from the analysis of the pA scattering data in the framework of the Dirac equation. There are no data available beyond a proton kinetic energy of 1 GeV. We assume in our calculations that for larger energies the momentum-dependent potential decreases according to our fit. This leads to uncertainties at higher beam energies. The reactions, which we study here, have a maximal beam energy of $E_{kin} = 1.5$ GeV.

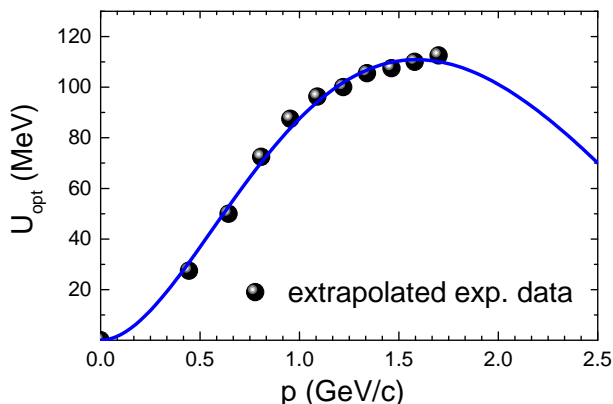


FIG. 1. Schrödinger equivalent optical potential U_{opt} versus total momentum p of the proton extracted from pA collisions [60, 61].

In a second step we have to get the two body interaction between two nucleons. The Schrödinger equivalent potential is obtained by averaging the two body potential $V(\mathbf{p}, \mathbf{p}_1)$ over the Fermi distribution of the cold target nucleons

$$U_{SEQ}(p) = \frac{\int^{p_F} V(\mathbf{p}, \mathbf{p}_1) dp_1^3}{\frac{4}{3}\pi p_F^3} \quad (2)$$

With $\Delta p = \sqrt{(\mathbf{p}_{01} - \mathbf{p}_{02})^2}$ we find that a functional form

$$V(\Delta p) = V(\mathbf{p}_{01}, \mathbf{p}_{02}) = (a\Delta p + b\Delta p^2) \exp[-c\sqrt{\Delta p}] \quad (3)$$

In the Dirac analysis the vector potentials depend linearly on the baryon density in the nucleus. Therefore we assume that the momentum-dependent part of the two body potential has also a linear dependence on the baryon density, and obtain finally:

$$V(\mathbf{r}_1, \mathbf{r}_2, \mathbf{p}_{01}, \mathbf{p}_{02}) = (a\Delta p + b\Delta p^2) \exp[-c\sqrt{\Delta p}] \delta(\mathbf{r}_1 - \mathbf{r}_2). \quad (4)$$

The δ function creates a linear density dependence. The energy of the system is

$$\begin{aligned} E &= \langle \psi(t) | (T + V) | \psi(t) \rangle \\ &= \sum_i \left[\langle i | \frac{p^2}{2m} | i \rangle + \sum_{i \neq j} \langle ij | V_{ij} | ij \rangle \right] \\ &= \int H(r) d^3r. \end{aligned} \quad (5)$$

$|\psi(t)\rangle = \prod_i |\psi_i\rangle$ is the n-body wave function, which is taken as the direct product of the single particle wave functions of the nucleons. The momentum-dependent potential has been introduced in QMD type transport approaches in Ref. [11] and explored later in Refs. [13, 20, 26, 63] and for BUU type approaches in Ref. [10] and has been widely applied later in different forms [12, 14–19, 64, 65].

To include a momentum-dependent interaction in a mean field approach is a challenging task and yield possibly other forces than in the QMD approach. This is discussed in Appendix A. This one has to keep in mind when comparing mean field (BUU) and QMD results.

The total potential energy of nucleons in PHQMD has three parts, a local static Skyrme type interaction, a local momentum-dependent interaction and a Coulomb interaction

$$\begin{aligned} V_{ij} &= V(\mathbf{r}_i, \mathbf{r}_j, \mathbf{r}_{i0}, \mathbf{r}_{j0}, \mathbf{p}_{i0}, \mathbf{p}_{j0}, t) \\ &= V_{\text{Skyrme loc}} + V_{\text{mom}} + V_{\text{Coul}} \\ &= \frac{1}{2} t_1 \delta(\mathbf{r}_i - \mathbf{r}_j) + \frac{1}{\gamma + 1} t_2 \delta(\mathbf{r}_i - \mathbf{r}_j) \rho_{int}^{\gamma-1}(\mathbf{r}_{i0}, \mathbf{r}_{j0}, t) \\ &\quad + V(\mathbf{r}_i, \mathbf{r}_j, \mathbf{p}_{i0}, \mathbf{p}_{j0}) + \frac{1}{2} \frac{Z_i Z_j e^2}{|\mathbf{r}_i - \mathbf{r}_j|}. \end{aligned} \quad (6)$$

In QMD we use a single-particle Wigner density of the nucleon wave function ψ_i , which is given by

$$f(\mathbf{r}_i, \mathbf{p}_i, \mathbf{r}_{i0}, \mathbf{p}_{i0}, t) = \frac{1}{\pi^3 \hbar^3} e^{-\frac{2}{L}(\mathbf{r}_i - \mathbf{r}_{i0}(t))^2} e^{-\frac{L}{2\hbar^2}(\mathbf{p}_i - \mathbf{p}_{i0}(t))^2}, \quad (7)$$

where the Gaussian width L is taken as $L = 2.16 \text{ fm}^2$. The total one-body Wigner density is the sum over the densities of all nucleons, whereas the $\psi(t)$ in eq. 5 is the n-body wave function, which is chosen in PHQMD as the direct product of the single particle wave functions. The corresponding single particle density at \mathbf{r} is obtained by integrating the single-particle Wigner density over momentum and summing up the contribution

of all nucleons:

$$\begin{aligned}\rho_{sp}(\mathbf{r}, t) &= \sum_i \int d\mathbf{p}_i f(\mathbf{r}, \mathbf{p}_i, \mathbf{r}_{i0}, \mathbf{p}_{i0}, t) \\ &= \sum_i \left(\frac{2}{\pi L}\right)^{3/2} e^{-\frac{2}{L}(\mathbf{r}-\mathbf{r}_{i0}(t))^2}.\end{aligned}\quad (8)$$

The expectation value of the potential energy V_{ij} , between the nucleons i and j is given by

$$\begin{aligned}\langle V_{ij}(\mathbf{r}_{i0}, \mathbf{p}_{i0}, \mathbf{r}_{j0}, \mathbf{p}_{j0}, t) \rangle &= \\ &= \int d^3r_i d^3r_j V_{ij}(\mathbf{r}_i, \mathbf{r}_j, \mathbf{p}_{i0}, \mathbf{p}_{j0}) \\ &\times f(\mathbf{r}_i, \mathbf{r}_{i0}, \mathbf{p}_{i0}, \mathbf{t}) f(\mathbf{r}_j, \mathbf{r}_{j0}, \mathbf{p}_{j0}, \mathbf{t}),\end{aligned}\quad (9)$$

and the interaction density is given by

$$\begin{aligned}\rho_{\text{int}}(\mathbf{r}_{i0}, t) &= \sum_{j \neq i} \int d^3r_i d^3r_j d^3p_i d^3p_j \delta(\mathbf{r}_i - \mathbf{r}_j) \\ &\times f(\mathbf{r}_i, \mathbf{p}_i, \mathbf{r}_{i0}, \mathbf{p}_{i0}, \mathbf{t}) f(\mathbf{r}_j, \mathbf{p}_j, \mathbf{r}_{j0}, \mathbf{p}_{j0}, \mathbf{t}).\end{aligned}\quad (10)$$

In order to extend PHQMD to relativistic energies we take into account the Lorentz contraction of the initial nuclei. This is done in an approximate way, as explained in Ref. [42], by introducing a modified single-particle Wigner density for each nucleon i :

$$\begin{aligned}\tilde{f}(\mathbf{r}_i, \mathbf{p}_i, \mathbf{r}_{i0}, \mathbf{p}_{i0}, t) &= \\ &= \frac{1}{\pi^3} e^{-\frac{2}{L}[\mathbf{r}_i^T(t) - \mathbf{r}_{i0}^T(t)]^2} e^{-\frac{2\gamma_{cm}^2}{L}[\mathbf{r}_i^L(t) - \mathbf{r}_{i0}^L(t)]^2} \\ &\times e^{-\frac{L}{2}[\mathbf{p}_i^T(t) - \mathbf{p}_{i0}^T(t)]^2} e^{-\frac{L}{2\gamma_{cm}^2}[\mathbf{p}_i^L(t) - \mathbf{p}_{i0}^L(t)]^2},\end{aligned}\quad (11)$$

which accounts for the Lorentz contraction of the nucleus in the beam z -direction in coordinate and momentum space by including $\gamma_{cm} = 1/\sqrt{1 - v_{cm}^2}$, where v_{cm} is the velocity of projectile and target in the computational frame, which is the center-of-mass system of the heavy-ion collision. Accordingly, the interaction density modifies as

$$\begin{aligned}\tilde{\rho}_{\text{int}}(\mathbf{r}_{i0}, t) &\rightarrow C \sum_j \left(\frac{1}{\pi L}\right)^{3/2} \gamma_{cm} e^{-\frac{1}{L}[\mathbf{r}_{i0}^T(t) - \mathbf{r}_{j0}^T(t)]^2} \\ &\times e^{-\frac{\gamma_{cm}^2}{L}[\mathbf{r}_{i0}^L(t) - \mathbf{r}_{j0}^L(t)]^2}.\end{aligned}\quad (12)$$

For the energies considered here the relativistic correction are not important.

B. Relation of the potential to the EoS of nuclear matter

In infinite nuclear matter, momentum and position are not correlated and one can calculate from the potential the equation-of-state of cold nuclear matter. In infinite matter the static part of the QMD potential is given, as in [42], by

$$V_{\text{Skyrme stat}} = \alpha \frac{\rho}{\rho_0} + \beta \left(\frac{\rho}{\rho_0}\right)^\gamma, \quad (13)$$

to this the momentum-dependent part for cold nuclear matter is added, which can be obtained by

$$V_{\text{mom}}(p_F) = \frac{\int^{p_F} \int^{p_F} dp_1^3 dp_2^3 V(\mathbf{p}_2 - \mathbf{p}_1) \frac{\rho}{\rho_0}}{\left(\frac{4}{3}\pi p_F^3\right)^2}. \quad (14)$$

The Fermi momentum is a function of the density and therefore one obtains the total strong interaction potential

$$V_{\text{Skyrme}}(\rho) = V_{\text{Skyrme stat}}(\rho) + V_{\text{mom}}(\rho). \quad (15)$$

To calculate the energy per nucleon, we introduce $U = \int V(\rho) d\rho$. This allow to write

$$\frac{E}{A}(\rho) = \frac{3}{5} E_{\text{Fermi}}(\rho) + \frac{U}{\rho}. \quad (16)$$

This equation contains the 3 parameters α, β, γ , which have to be determined. Two of them can be obtained by the requirement that at normal nuclear density $E/A = -16$ MeV. The third parameter is traditionally determined by fixing the compression modulus K of nuclear matter, the inverse of the compressibility $\chi = \frac{1}{V} \frac{dV}{dP}$, which corresponds to the curvature of the energy at $\rho = \rho_0$ (for $T = 0$):

$$K = 9\rho \left. \frac{dP}{d\rho} \right|_{\rho=\rho_0} = 9\rho^2 \left. \frac{\partial^2 (E/A(\rho))}{(\partial\rho)^2} \right|_{\rho=\rho_0}. \quad (17)$$

Here P is the pressure of the system ($P = \rho^2 \frac{\partial E/A}{\partial \rho}$). An EoS with a rather low value of the compression modulus K yields a weak repulsion against the compression of nuclear matter and thus describes "soft" matter (denoted by "S"). A high value of K causes a strong repulsion of nuclear matter under compression (called a hard EoS, "H"). The hard, the soft and the soft momentum-dependent equations-of-state used in this study are illustrated in Fig. 2 and the parameters for the three equations-of-state are presented in Table I. Soft and soft momentum-dependent EoS have for cold nuclear matter the same $\frac{E}{A}(\rho)$.

EoS	α [MeV]	β [MeV]	γ	K [MeV]
S	-383.5	329.5	1.15	200
H	-125.3	71.0	2.0	380
SM	-478.87	413.76	1.1	200
a [MeV ⁻¹] b [MeV ⁻²] c [MeV ⁻¹] 236.326 -20.73 0.901				

TABLE I. Parameters of the potential used in PHQMD.

C. QMD Propagation

For the time evolution of the wave function we use the Dirac-Frenkel-McLachlan approach [66, 67], which is

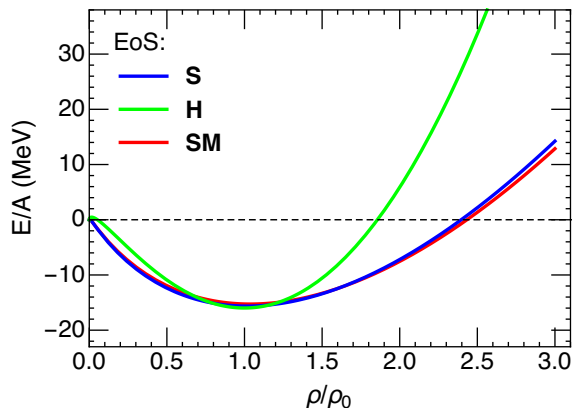


FIG. 2. Equation-of-state for $T = 0$ for the hard (green line), soft (blue line) and the soft momentum-dependent potential (red line).

based on the variation

$$\delta \int_{t_1}^{t_2} dt \langle \psi(t) | i \frac{d}{dt} - H | \psi(t) \rangle = 0 \quad (18)$$

and has been developed in chemical physics. It has also been applied in nuclear physics for QMD like models [13, 53, 68, 69]. This approach provides the time derivatives of the centers of the wave functions $\mathbf{r}_{i0}, \mathbf{p}_{i0}$. Being a n-body approach it conserves the correlations in the system and does not suppress fluctuations as mean-field calculations do. Since clusters are n-body correlations it is well suited to address their creation and time evolution. With our assumption that the wave functions have a Gaussian form and that the width of the wave function is time independent, one obtains for the time evolution of the centroids of the Gaussian single particle Wigner density two equations, which resemble the equation-of-motion of a classical particle with the phase space coordinates $\mathbf{r}_{i0}, \mathbf{p}_{i0}$ [13]. The difference is that here the expectation value of the quantal Hamiltonian is used and not a classical Hamiltonian:

$$\dot{r}_{i0} = \frac{\partial \langle H \rangle}{\partial p_{i0}} \quad \dot{p}_{i0} = -\frac{\partial \langle H \rangle}{\partial r_{i0}} \quad (19)$$

The Hamiltonian of the nucleus is the sum of the Hamiltonians of the nucleons, composed of kinetic and two-body potential energy, which has a strong interaction and a Coulomb part

$$H = \sum_i H_i = \sum_i (T_i + \sum_{j \neq i} V_{ij}). \quad (20)$$

The expectation value of the Coulomb interaction can also be calculated analytically. The expectation value of

the Hamiltonian which enters Eq. 19 is finally given by

$$\langle H \rangle = \langle T \rangle + \langle V \rangle \quad (21)$$

$$= \sum_i (\sqrt{p_{i0}^2 + m^2} - m) \quad (22)$$

$$+ \sum_i \langle V_{Skyrme}(\mathbf{r}_{i0}, t) + V_{mom}(\mathbf{r}_{i0}, \mathbf{p}_{i0}t) + V_{coul}(\mathbf{r}_{i0}, t) \rangle.$$

D. Cluster production in PHQMD

In the PHQMD 3 mechanisms for the dynamical clusters production are available:

1) **potential mechanism:** The attractive potential between baryons with a small relative momentum keeps them close together and can lead to a group of bound nucleons. Such groups of comoving nucleons can be identified as clusters during the dynamical evolution, using the advanced Minimum Spanning Tree (aMST) method, as detailed in Ref. [44]. The MST [13] collects nucleons which are close in coordinate space. At a given time t a snapshot of the positions and momenta of all nucleons is recorded and the MST clusterization algorithm is applied: two nucleons i and j are considered as “bound” to a deuteron or to a larger cluster $A > 2$ if they fulfill the condition

$$|\mathbf{r}_i^* - \mathbf{r}_j^*| < r_{clus}, \quad (23)$$

where on the left hand side the positions are boosted in the center-of-mass of the ij pair. The maximal distance between cluster nucleons, $r_{clus} = 4$ fm, corresponds roughly to the range of the attractive NN potential. Additionally, in aMST the clusters have to have a negative binding energy $E_B < 0$. It is important to highlight that MST serves as a tool for cluster recognition, not a mechanism for ‘building’ clusters, since the QMD transport model propagates baryons and not pre-formed clusters.

2) **kinetic mechanism:** Deuterons can be created in catalytic hadronic reactions as $\pi NN \leftrightarrow \pi d$ and $NNN \leftrightarrow Nd$ in different isospin channels. The quantum nature of the deuteron is considered through an excluded volume which forbids its production if another hadron is localized in this volume. We project furthermore the relative momentum of the incoming nucleons onto the deuteron wave function in momentum space. These quantum corrections lead to a significant reduction of deuteron production by kinetic mechanism, particularly at target/projectile rapidities. We note that the kinetic deuterons are propagated explicitly in the PHQMD as a degree-of-freedom (contrary to the nucleons in MST clusters, which are propagated as nucleons. We refer the reader to Ref. [44] for the details.

3) **coalescence mechanism:** Additionally to the dynamical cluster production by potential interaction and kinetic reactions occurring during the whole time evolution of the system, we have an option in PHQMD to apply a coalescence procedure at the freeze-out time of

the nucleons. We recall that the coalescence framework in PHQMD is adopted from UrQMD [40] and described in Ref. [41]. A proton and a neutron can form a deuteron if their distance at the time, when the last one of the two freezes out, in phase space is less than (see Ref. [41]) $|r_1 - r_2| \leq 3.575$ fm and $|p_1 - p_2| \leq 285$ MeV/c. These radii have been fitted to data in order to reproduce the deuteron multiplicity, if a spin degeneracy factor of $3/8$ [41] is applied as in UrQMD [40]. Since the coalescence procedure can be applied to the same events in which the clusters can be identified by aMST it provides a unique possibility for the direct comparison of the both production mechanisms within the same code.

III. CONSEQUENCES OF THE EOS FOR HEAVY-ION DYNAMICS AT SIS ENERGIES

Before we compare the PHQMD results to the experimental data we discuss how the bulk properties in heavy-ion collisions depend on the different EoS. To demonstrate this we use Au+Au collisions at $E_{kin} = 1.5$ A GeV. We start with the maximum density attained during the collision.

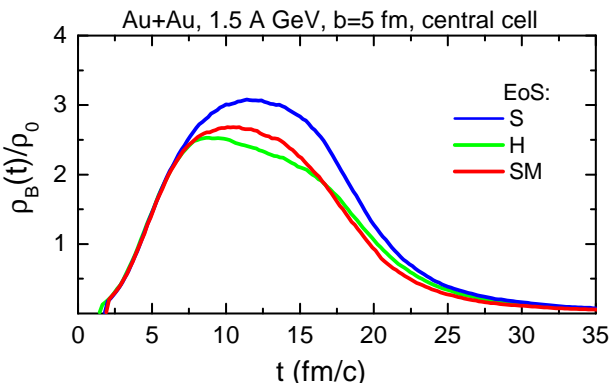


FIG. 3. Time evolution of the normalized baryon density distributions in the central cell for Au+Au collisions at $b = 5$ fm and $E_{kin} = 1.5$ A GeV. The blue lines "S" correspond to the PHQMD calculations with the "soft" EoS, the green lines "H" show the "hard" EoS, the red lines the "SM" represent the momentum-dependent "soft" EoS.

In Fig. 3 we show the time evolution of the normalized baryon density (to $\rho_0 = 0.168$ nucleons/fm³) in the central cell in Au+Au collisions for $b = 5$ fm at $E_{kin} = 1.5$ A GeV. The calculations are done for three different EoS: the blue lines "S" correspond to PHQMD calculations with the "soft" EoS, the green lines "H" show the "hard" EoS, the red lines "SM" represent the "momentum-dependent soft" EoS. One can see that the baryon density in the central cell does not only depend on the compression modulus - which determines whether an equation-of-state is soft or hard - but also on the momentum-dependence of the potential. Despite of being soft, the maximal density for the soft momentum-

dependent EoS is very close to that obtained for a hard EoS and much lower than that for a soft EoS without momentum-dependence. This has of course consequences for the mean free path and quantities, which characterize the collisions as directed flow v_1 .

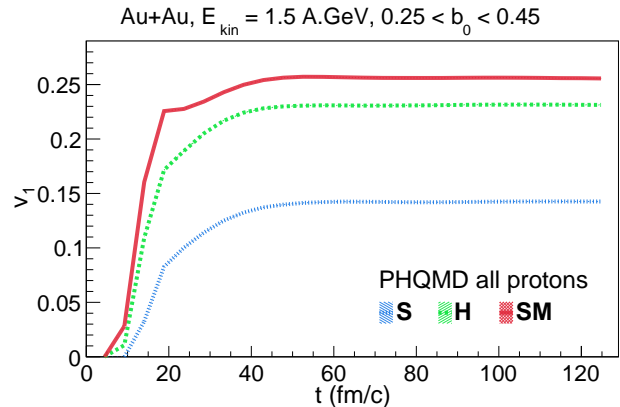


FIG. 4. v_1 of all protons (free and bound in MST clusters) for Au+Au collisions at $E_{kin} = 1.5$ A GeV for centrality $0.25 < b_0 < 0.45$ as a function of time. The blue line "S" corresponds to the PHQMD "soft" EoS, the green line "H" - to the "hard" EoS, the red line "SM" represents the momentum-dependent "soft" EoS.

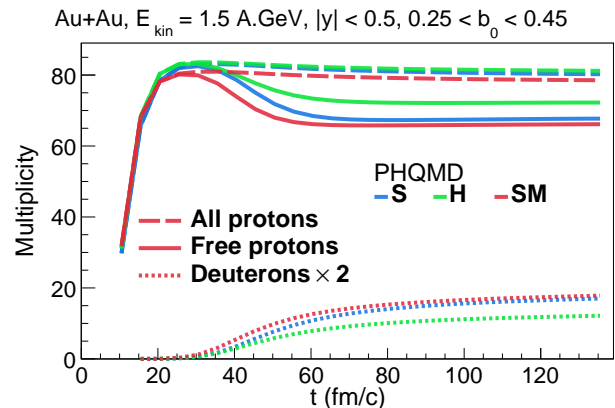


FIG. 5. Time evolution of the midrapidity multiplicities of the protons and deuterons for Au+Au collisions at $E_{kin} = 1.5$ A GeV for centrality $0.25 < b_0 < 0.45$. The solid lines are for the free unbound protons, the long dashed lines show all (free + bound) protons, the short dashed lines present deuterons. The deuteron lines are multiplied by a factor of 2 for better visibility. The blue line "S" corresponds to the PHQMD "soft" EoS, the green line "H" - to the "hard" EoS, the red line "SM" represents the momentum-dependent "soft" EoS.

The azimuthal distribution of nucleons at the end of a heavy-ion collisions can be analyzed by a Fourier series with the flow coefficient v_n , defined by

$$\frac{dN}{d\phi} \propto 1 + 2v_1 \cos(\phi - \Psi_R) + 2v_2 \cos(2(\phi - \Psi_R)) + \dots \quad (24)$$

ϕ is the azimuthal angle of the particle measured with respect to the event plane (or a "reaction plane") Ψ_R . The flow coefficients v_n , $n = 1, 2, \dots$ are defined with respect to Ψ_R as average over all particles in all events for a given centrality range [70, 71]:

$$v_n = \langle \cos(n(\phi - \Psi_R)) \rangle. \quad (25)$$

In Fig. 4 we present the time evolution of v_1 (for $\Psi_R = 0$) for all protons (free and bound in clusters) for the three EoS in the FOPI mid-centrality interval ($0.25 < b_0 = b/b_{max} < 0.45$) integrated over $y > 0$ and p_T . One can see that v_1 for the soft EoS is considerably smaller than that for the SM EoS, which is close to that for a hard EoS. For SM v_1 develops also earlier when the two nuclei touch each other and before the system has reached its maximum density. v_1 for the hard EoS starts slightly later when the system gets compressed. H and SM have almost the same time profile although due to very different origins: Whereas for the hard EoS it is the density gradient which creates the in-plane flow, for the SM EoS, which has a density gradient similar to the soft EoS, it is the momentum-dependence of the potential, which is at the origin for the increase of v_1 . v_1 of the S EoS develops later and does not reach the same maximal value due to smoother density gradients.

This can be further illustrated by showing in Fig. 5 the time evolution of the midrapidity multiplicities of the protons and deuterons for Au+Au collisions at $E_{kin} = 1.5$ A GeV for the centrality $0.25 < b_0 < 0.45$. Here the solid lines are for the unbound protons, the long dashed lines show all (unbound + bound) protons, the short dashed lines present deuterons. We see that the number of deuterons stabilizes after freeze out and that the number of deuteron for a S and SM EoS are very similar and distinct from that of H EoS.

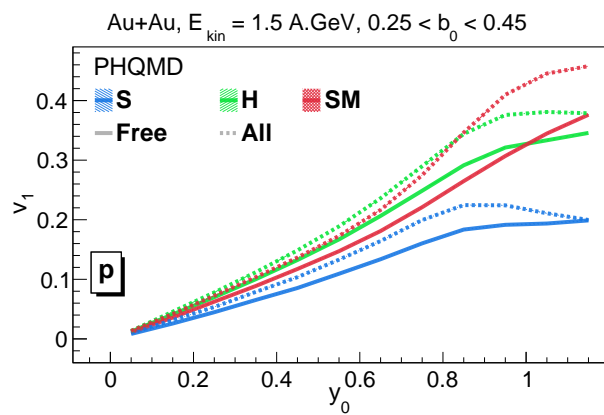


FIG. 6. v_1 of protons versus y_0 for Au+Au collisions at $E_{kin} = 1.5$ A GeV for the impact parameter range $0.25 < b_0 < 0.45$. The blue line "S" corresponds to the PHQMD "soft" EoS, the green line "H" - to the "hard" EoS, the red line "SM" represents the momentum-dependent "soft" EoS. The solid lines are for the free unbound protons, while the dashed lines show all (free + bound) protons.

A second general observation concerns the in-plane flow of clusters: we observe that the p_T integrated in-plane flow, v_1 , of finally unbound protons is smaller than v_1 of all (free + bound in clusters) protons for all 3 EoS. This is shown, as a function of $y_0 = y/y_{beam}$, in Fig. 6, which displays v_1 for Au+Au collisions at $E_{kin} = 1.5$ A GeV in the impact parameter range $0.25 < b_0 < 0.45$. This observation contradicts the assumption that the phase space distribution of clusters, which contain N nucleons, is just a single proton distribution to the N 'th power and taken at a momentum p/N : $f^N(p) = [f(p/N)]^N$.

It can be understood as follows: v_1 of protons depends on the position where they are located during the heavy-ion collision. Those which are located at the transition between participant and spectator region, where the density gradient is large, have the highest value of v_1 whereas for those which are at the center of the reaction, v_1 is close to zero. v_1 created at the intersection between the participant and spectator region is - by subsequent collisions and the potential - shared with spectator nucleons. They have the tendency to stay together and to form spectator fragments, which have consequently a large v_1 . The difference of v_1 between free and all protons at forward rapidity reflects therefore the lower probability to find there nucleons coming from the participant regions for clusters.

A third general observation is that the rapidity spectra and the slope of mid-rapidity p_T -spectra depend on the EoS. This is shown in Figs. 7 and 8, which display, from top to bottom, the rapidity distributions and p_T -spectra of free protons, deuterons for mid-rapidity Au+Au collisions at $E_{kin} = 1.5$ A GeV and a compilation of free protons (yellow), deuterons (magenta), tritons (green) and 3He (blue) in a logarithmic scale. S, H and SM are presented by dotted, dashed and full lines, respectively. The larger the mass of the cluster the broader becomes the distribution. This indicates that the spectator matter produces clusters more frequently than the participant matter. We see here again that the S and SM EoS produce about the same number of deuterons and about 30% more than calculations with a hard EoS. As follows from Fig. 7, the momentum-dependence of the EoS has small influence on particles emitted close to midrapidity, which originate from a fireball with a temperature of about $T \sim 100$ MeV. There, due to the same compressibility, S and SM behave similarly. As shown in the bottom plot of Fig. 7, this lower multiplicity for a hard EoS is also visible for larger clusters. S and SM produce around 30% more $A = 3$ clusters than H. The sensitivity to EoS is also visible in the slope of p_T -spectra as shown in Fig. 8. The S EoS leads to much softer transverse spectra of protons and light clusters compared with the SM EoS and H EoS. We can conclude these general observations with the remark that, depending on the observables, the results of calculations with SM can be close to that of H or close to that of S. This offers the possibility, by comparing a multitude of observables, to

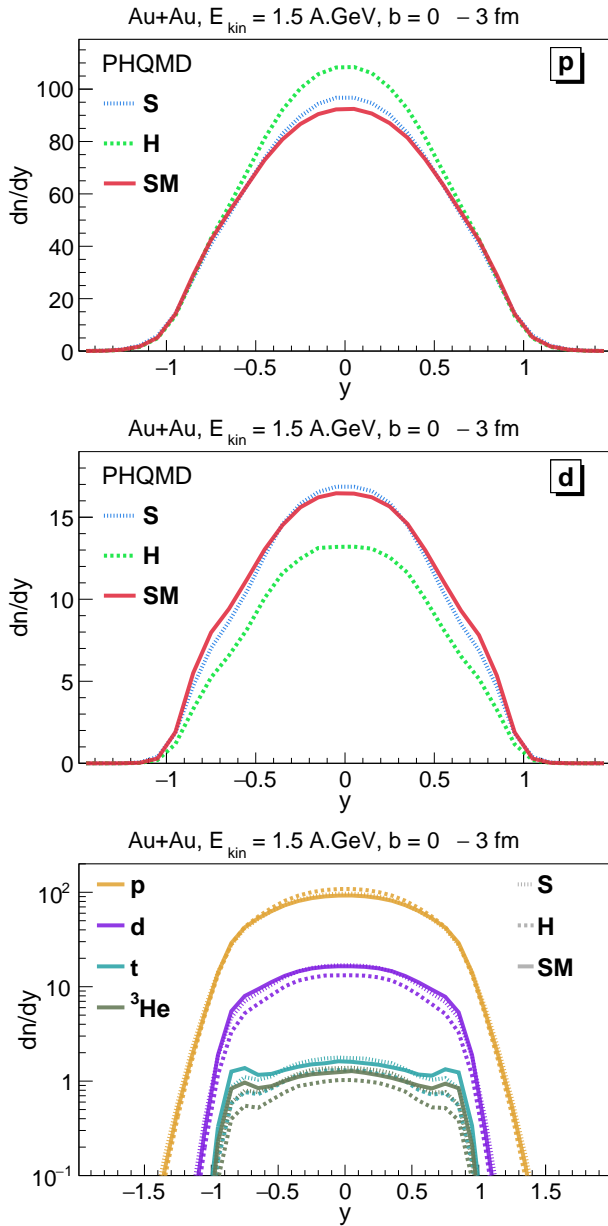


FIG. 7. Rapidity distribution dN/dy of protons (upper), deuterons (middle) and compilation of protons, deuterons, tritons and ${}^3\text{He}$ for Au+Au collisions at $E_{kin} = 1.5$ A GeV for the impact parameter range $0 < b < 3$ fm. The dotted lines "S" correspond to the PHQMD "soft" EoS, the dashed lines "H" – to the "hard" EoS, the solid lines "SM" represent the momentum-dependent "soft" EoS.

determine experimentally the momentum and density dependence of the EoS.

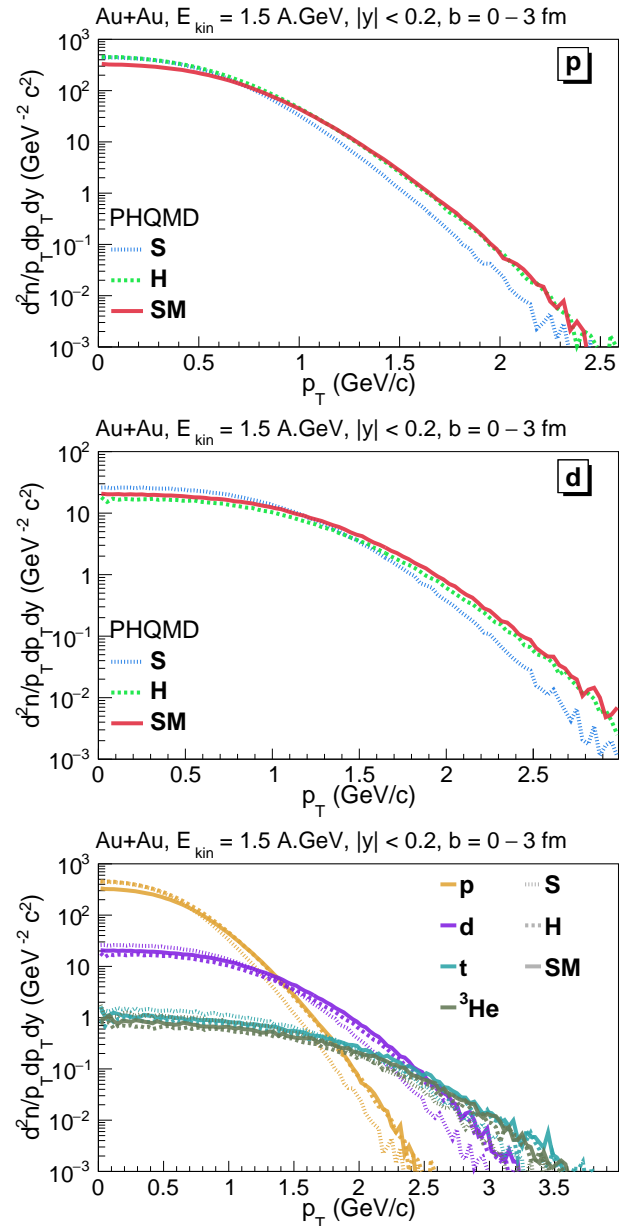


FIG. 8. Invariant p_T spectra of protons (upper), deuterons (middle) and compilation of protons, deuterons, tritons and ${}^3\text{He}$ for mid-rapidity ($|y| < 0.2$) Au+Au collisions at $E_{kin} = 1.5$ A GeV for the impact parameter range $0 < b < 3$ fm. The dotted lines "S" correspond to the PHQMD "soft" EoS, the dashed lines "H" – to the "hard" EoS, the solid lines "SM" represent the momentum-dependent "soft" EoS.

IV. THE PHQMD RESULTS IN COMPARISON TO EXPERIMENTAL DATA

A. Directed and elliptic flow

We start now with the comparison of our PHQMD calculation with experimental observables. In this study we concentrate on the comparison of the PHQMD re-

sults with the fixed target experiments at SIS energies, HADES and FOPI, which have the advantage that they can define the reaction plane with high accuracy due to the HADES forward wall detector [49], and the FOPI 4π geometry [28]. We study the directed flow, v_1 , and the elliptic flow, v_2 for Au+Au collisions, at three different but neighboring energies around $E_{kin} \simeq 1.2$ GeV.

While in the theoretical model calculations the geometry of each collision is well defined because the reaction plane is linked to the coordinate system (i.e. $\Psi_R = 0$), this is not the case for experiments, which measure only a subset of the final hadrons in a selected part of the phase-space. They are used to experimentally define the so-called event plane angle Ψ_{EP} , which has a dispersion around the ideal reaction plane angle Ψ_R . However, this dispersion can be estimated from data and is used to correct the measured raw flow coefficients. There are different methods employed to extract these corrections [70, 71]; they might affect the flow v_n at large p_T in different ways (cf. the study within the PHSD model in Ref. [72]).

In this study we calculate the flow coefficients using the theoretically defined reaction plane ($\Psi_R = 0$) and compute the directed and elliptic flow as

$$v_1 = \langle \frac{p_x}{p_T} \rangle, \quad v_2 = \langle \frac{p_x^2 - p_y^2}{p_T^2} \rangle \quad (26)$$

where p_T is the transverse momentum $p_T = (p_x^2 + p_y^2)^{1/2}$ of the hadron with 4-momentum $p = (E, p_x, p_y, p_z)$.

B. Directed flow v_1

The first coefficient v_1 , the directed flow, measures the deflection of the projectile and target nucleons towards a finite value of p_x , where x is the direction of the impact parameter. The value of p_x is (per definition) positive for particles with a positive rapidity and negative for those with a negative rapidity. As discussed, the finite v_1 can have two origins: either the high density overlap zone of projectile and target creates forces in transverse direction or the momentum-dependent interaction deviates projectile and target in transverse direction. The former happens when a high density is reached, the second when projectile and target start to overlap and therefore the momentum-dependent potential is strongest.

1. Comparison of the PHQMD v_1 to the HADES data

We start with the comparison of the PHQMD results for the directed flow v_1 of protons and light clusters with the experimental data from the HADES Collaboration [49] for Au+Au collisions at $E_{kin} = 1.23$ A GeV ($\sqrt{s_{NN}} = 2.4$ GeV). We note that with "protons" we mean only "free" protons (if not specified explicitly), i.e. those which are not bound in clusters.

In Fig. 9 we show the PHQMD results for the directed flow v_1 of protons as a function of rapidity y for different p_T intervals for 20-30% central Au+Au collisions at $E_{kin} = 1.23$ A GeV and for different p_T cuts in comparison to the HADES experimental data from Ref. [49]. The PHQMD calculations are done for three different equations-of-state summarized in table I. In this plot and in all the following plots the blue lines "S" correspond to the PHQMD calculations with the "soft" EoS, the green lines "H" show the "hard" EoS, the red lines "SM" represent the momentum-dependent "soft" EoS; the colored areas represent the statistical errors. Both, the theoretical as well as the experimental rapidity distributions of v_1 , are rather insensitive to the chosen p_T interval. The soft momentum-dependent EoS gives even a steeper slope than the hard EoS and comes closest to the experimental data. The slope of the calculations with a soft EoS is incompatible with the experimental data. We note that the soft and hard EoS have been chosen as a boundary of the values for the compressibility, which has been obtained from studies of monopole vibrations [73], which are sensitive to densities around normal nuclear matter density, and early Plastic Ball data [1], which are sensitive to much higher densities and could be explained by a larger compressibility modulus [21].

In Fig. 10 we present the PHQMD results for $v_1(y)$ of protons (top left), deuterons (bottom left) and tritons (top right) in comparison to the HADES experimental data [48] for Au+Au collisions at $E_{kin} = 1.23$ A GeV for the p_T interval $1.0 < p_T < 1.5$ GeV/c for hard, soft and momentum-dependent EoS. In the bottom right figure we display $v_1(y)$ separately for two mechanisms of deuteron production: kinetic (yellow) and MST (violet).

Fig. 10 shows that the increase of the slope of $v_1(y)$ with the size of the cluster, discussed in section III, is confirmed experimentally. This points towards a formation of the deuterons close to the border of the overlap region between projectile and target, where v_1 of nucleons is highest. Some of these PHQMD results are in line with early findings in Ref. [11] and confirm recent calculations in Refs. [26, 65]. Also for clusters the inclusion of the momentum-dependent interaction in a S EoS gives even a steeper slope than a hard EoS and the results come closer to the HADES experimental data. The calculations reproduce also the slight non linear dependence of $v_1(y)$ at large rapidities. The directed flow is rather similar for kinetic and MST deuterons (bottom right). Both show about the same $v_1(y)$. The slope of $v_1(y)$ for tritons is still higher than that for deuterons and even a soft momentum-dependent interaction underpredicts noticeable the slope.

In Fig. 11 we show the p_T dependence of v_1 of protons for 20-30% central Au+Au collisions at $E_{kin} = 1.23$ A GeV for different rapidity bins - $-0.25 < y < -0.15$ (upper) and $-0.65 < y < -0.55$ (lower) - calculated for three EoS. One can see that the value of $v_1(p_T)$ increases with increasing rapidity for all EoS, keeping the hierarchy - soft, hard, momentum-dependent soft EoS. One can

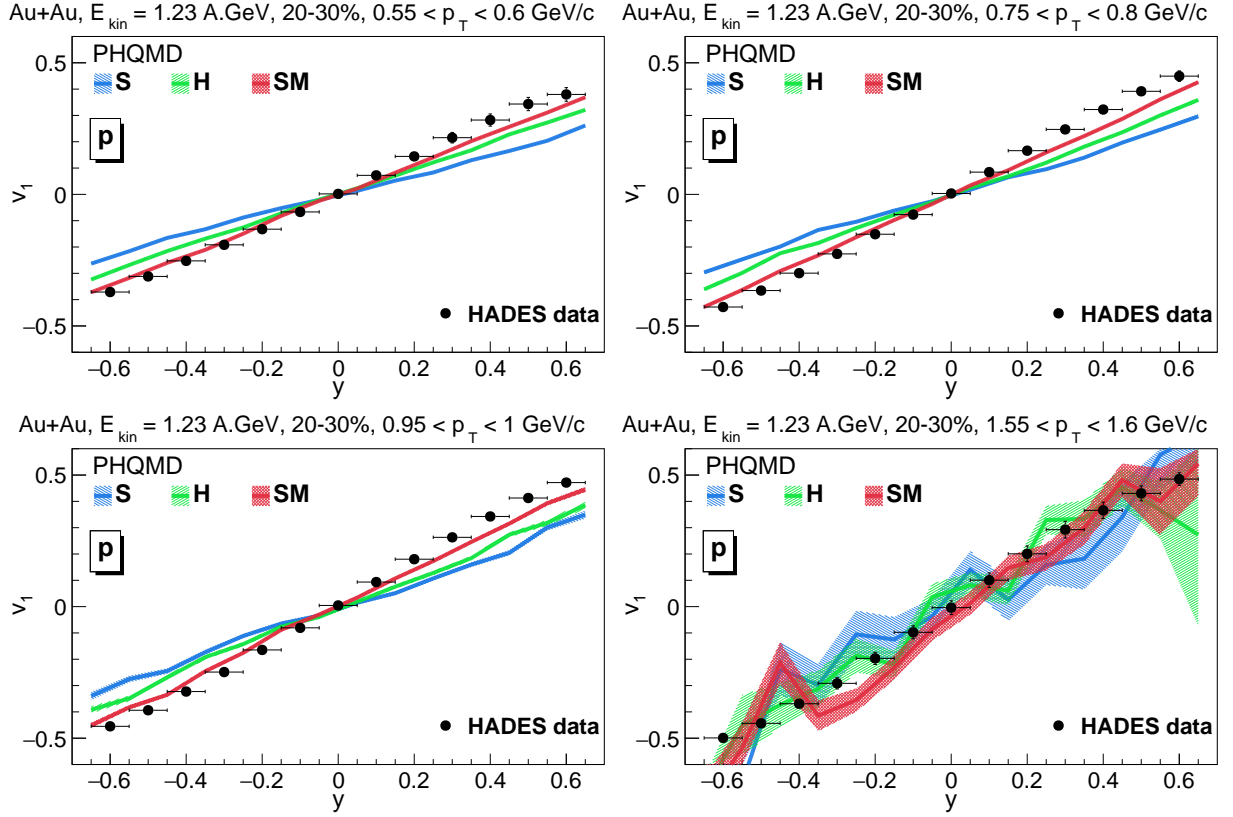


FIG. 9. The directed flow v_1 of protons as a function of rapidity y for different p_T intervals for 20-30% central Au+Au collisions at $E_{kin} = 1.23$ A GeV for different p_T intervals: $0.55 < p_T < 0.6$ GeV/c (upper left), $0.75 < p_T < 0.8$ GeV/c (upper right), $0.95 < p_T < 1.0$ GeV/c (lower left), $1.55 < p_T < 1.6$ GeV/c (lower right). The blue lines "S" correspond to the PHQMD calculations with the "soft" EoS, the green lines "H" show the "hard" EoS, the red lines the "SM" represent the momentum-dependent "soft" EoS. The height of the filled areas represent the statistical errors. The HADES experimental data are taken from Ref. [49].

also see that the SM EOS provides the best description of the HADES experimental data.

A similar behaviour of $v_1(p_T)$ holds for the light clusters as demonstrated in Fig. 12, which shows the p_T dependence of the directed flow of deuterons (top) and tritons (bottom) for the rapidity bin $-0.25 < y < -0.15$. One can see that the directed flow $v_1(p_T)$ for the hard EoS and SM EoS are closer to each other compared to the corresponding proton case in Fig. 11 (middle), however, well below the soft EoS, which substantially underestimates the experimental data.

2. Comparison of the PHQMD v_1 to the FOPI data

Now we step to a comparison of the PHQMD results for the directed flow for Au+Au collisions at $E_{kin} = 1.2$ and 1.5 A GeV with the FOPI data [50]. The FOPI Collaboration presents the results using the following kinematic variables:

- scaled rapidity y_0 :

$$y_0 = \frac{y}{y_{proj}}, \quad \text{where } y = \frac{1}{2} \log \left(\frac{E + p_z}{E - p_z} \right)$$

is the rapidity of a particle with energy E and 3-momentum $\mathbf{p} \equiv p$,

$$y_{proj} = \frac{1}{2} \log \left(\frac{E_P + P_P}{E_P - P_P} \right)$$

is the projectile rapidity and E_P , $P_P = P_{P,z}$ are the energy and momentum of the initial projectile nucleon in center-of-mass system;

- scaled transverse momentum u_{t0} :

$$u_{t0} = \frac{u_T}{u_{proj}},$$

where $u_T = \beta_T \gamma$ is the transverse velocity of a particle with velocity $\beta = p/E$, $\gamma = 1/\sqrt{1 - \beta^2}$ and $\beta_T = p_T/E$, while the projectile velocity is $u_{proj} = \beta_P \gamma_P$ with $\beta_P = P_P/E_P$.

- the centrality is defined in terms of the scaled impact parameter $b_0 = b/b_{max}$ with $b_{max} = 1.15(A_P^{1/3} + A_T^{1/3})$ fm, where A_P, A_T are the atomic numbers of projectile (P) and target (T).

The FOPI measurement of v_1 covers different sub-regions in the (y_0, u_{t0}) plane. Here we present the PHQMD results for $v_1(y_0)$ for $u_{t0} > 0.4$ and for $v_1(u_{t0})$ for $0.4 < |y_0| < 0.8$ for the centrality bin $0.25 < b_0 < 0.45$ ($3.34 < b < 6.022$ fm).

Figs. 13 and 14 show the directed flow v_1 of protons, deuterons, $A = 3$ clusters and ${}^4\text{He}$ as a function of y_0 for Au+Au collisions at $E_{kin} = 1.2$ and 1.5 A GeV, respectively, for $u_0 > 0.4$ and the impact parameter range $0.25 < b_0 < 0.45$ ($3.34 < b < 6.022$ fm) in comparison to the FOPI experimental data [50]. One can see that for all clusters as well as for protons the soft EoS underestimates also the FOPI data. The difference between the

hard and the soft momentum-dependent EoS are small for $u_{t0} > 0.4$ and the hard EoS leads to slightly larger v_1 , in contradistinction to the calculation for the HADES data Fig. 10.

That these findings are not trivial is shown in the bottom panel of Figs. 13 and 14, which display $v_1(y_0)$ for a SM EoS for different cluster sizes in comparison with the experimental results. We observe a strong dependence of the slope of $v_1(p_T)$ on the cluster size, which has been discussed in section III and which is indeed seen in the experimental data.

In Figures 15 and 16 we present the PHQMD results for v_1 of protons, deuterons, $A = 3$ and ${}^4\text{He}$ as a function of u_{t0} for Au+Au collisions at $E_{kin} = 1.2$ and 1.5 A GeV, respectively, for $0.4 < y_0 < 0.8$ and the impact parameter range $0.25 < b_0 < 0.45$ in comparison to the FOPI data from [50]. We note that the FOPI data were measured in a positive rapidity hemisphere. However, we reflect the FOPI data $v_1(u_{t0}) \rightarrow -v_1(u_{t0})$ for the better comparison to the HADES results. One can see a splitting of $v_1(u_{t0})$ with EoS, however, the behaviour is not monotonic - at low u_{t0} v_1 with the hard EoS is larger while at large u_{t0} the SM EoS gives larger v_1 for protons; this tendency is seen also for clusters. This is summarized on the lower plot for the SM EoS.

As follows from Figs. 13 - 16, the PHQMD calculations provide a qualitative description of the experimental data also for the FOPI data in rapidity as well as in u_{t0} . The form of the different $v_1(u_{t0})$ and $v_1(y_0)$ spectra at $E_{kin} = 1.2$ and 1.5 GeV are similar, in theory as well as in experiment, and the deviations between theory and experiment are also almost energy independent. Also the FOPI data show that $v_1(u_{t0})$ and $v_1(y_0)$ depend substantially on the cluster size. This is as well reproduced by PHQMD calculations. Despite of the different centralities, the different observables and the different acceptance ranges, one might compare the calculations for the HADES and FOPI data and come to the conclusions that for all cluster sizes the theoretical $v_1(y), v_1(y_0)$ and $v_1(p_T), v_1(u_{t0})$ calculations with SM are slightly below the data in all these experiments.

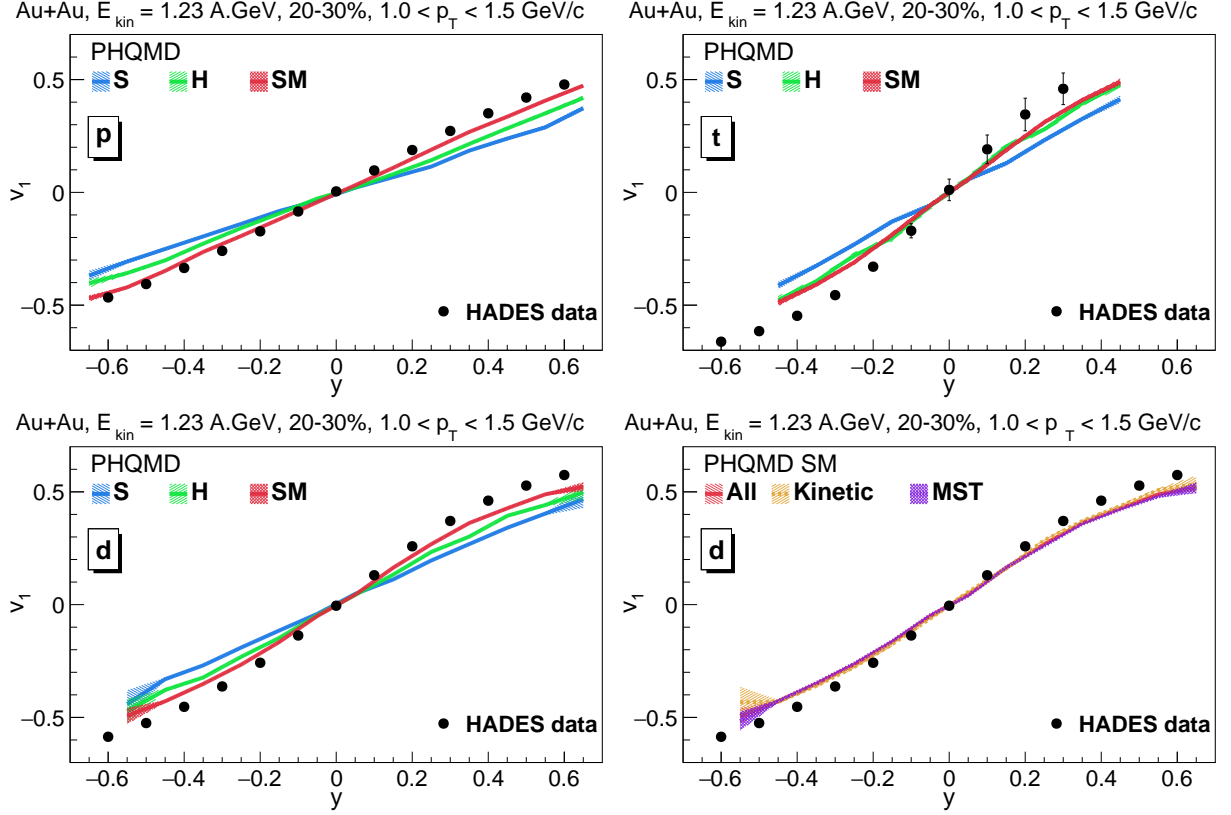


FIG. 10. v_1 of protons (upper left) and deuterons (lower row) and tritons (upper right) as a function of rapidity for 20-30% central Au+Au collisions at $E_{kin} = 1.23$ A GeV for $1.0 < p_T < 1.5$ GeV/c. The blue lines "S" correspond to the PHQMD calculations with the "soft" EoS, the green lines "H" show the "hard" EoS, the red lines "SM" represent the momentum-dependent "soft" EoS. The low right plot shows the $v_1(y)$ of deuterons for the SM EoS produced by different mechanisms: kinetic (yellow line), MST (violet line) as well as the $v_1(y)$ of all deuterons (red line, identical to the SM result on the lower left plot). The HADES experimental data are taken from Ref. [48].

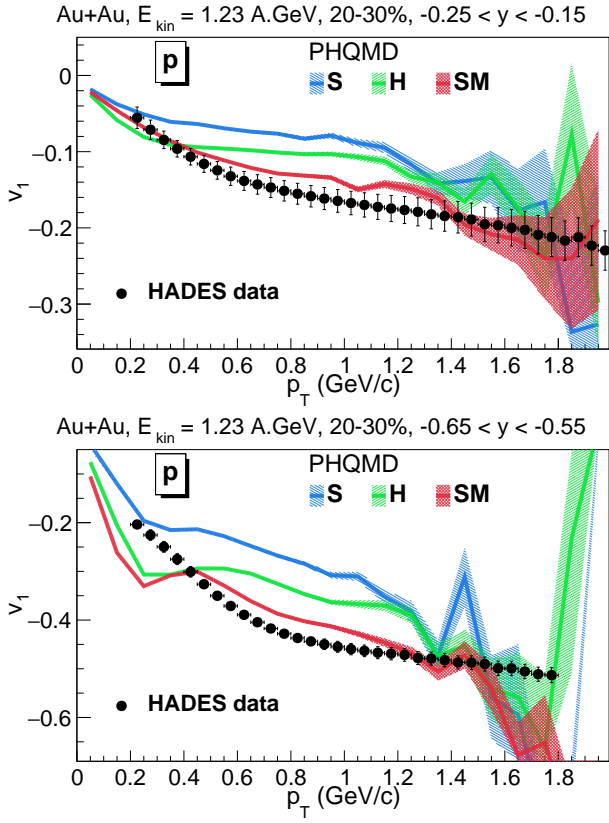


FIG. 11. v_1 of protons as a function of p_T for 20-30% central Au+Au collisions at $E_{kin} = 1.2$ A GeV for different rapidity bins: $-0.25 < y < -0.15$ (upper plot) and $-0.65 < y < -0.55$ (lower plot). The blue line "S" corresponds to the PHQMD "soft" EoS, the green line "H" – to the "hard" EoS, the red line "SM" represents the momentum-dependent "soft" EoS. The experimental data are taken from Ref. [49].

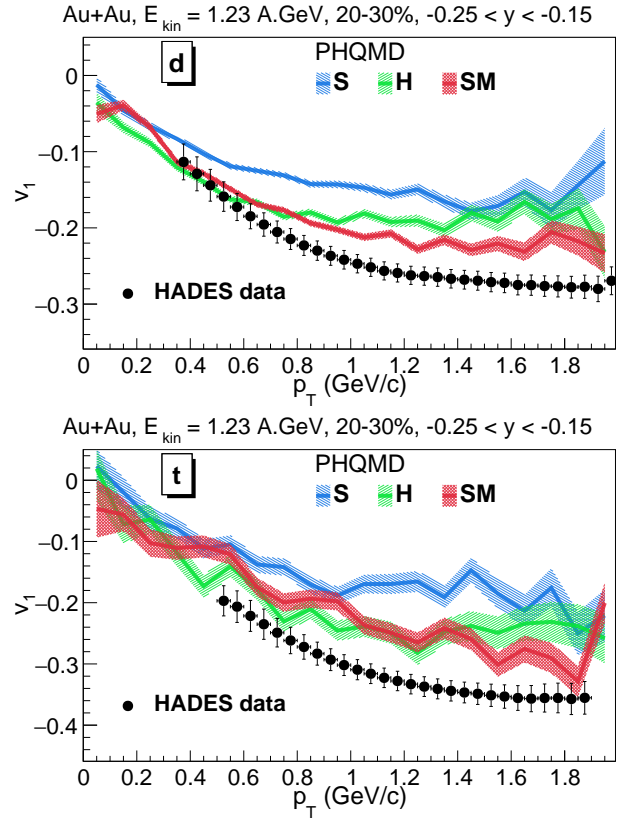


FIG. 12. v_1 of deuterons (upper plot) and tritons (lower plot) as a function of p_T for 20-30% central Au+Au collisions at $E_{kin} = 1.2$ A GeV in the rapidity bin $-0.25 < y < -0.15$. The color scheme is the same as in Fig. 11. The experimental data are taken from Ref. [49].

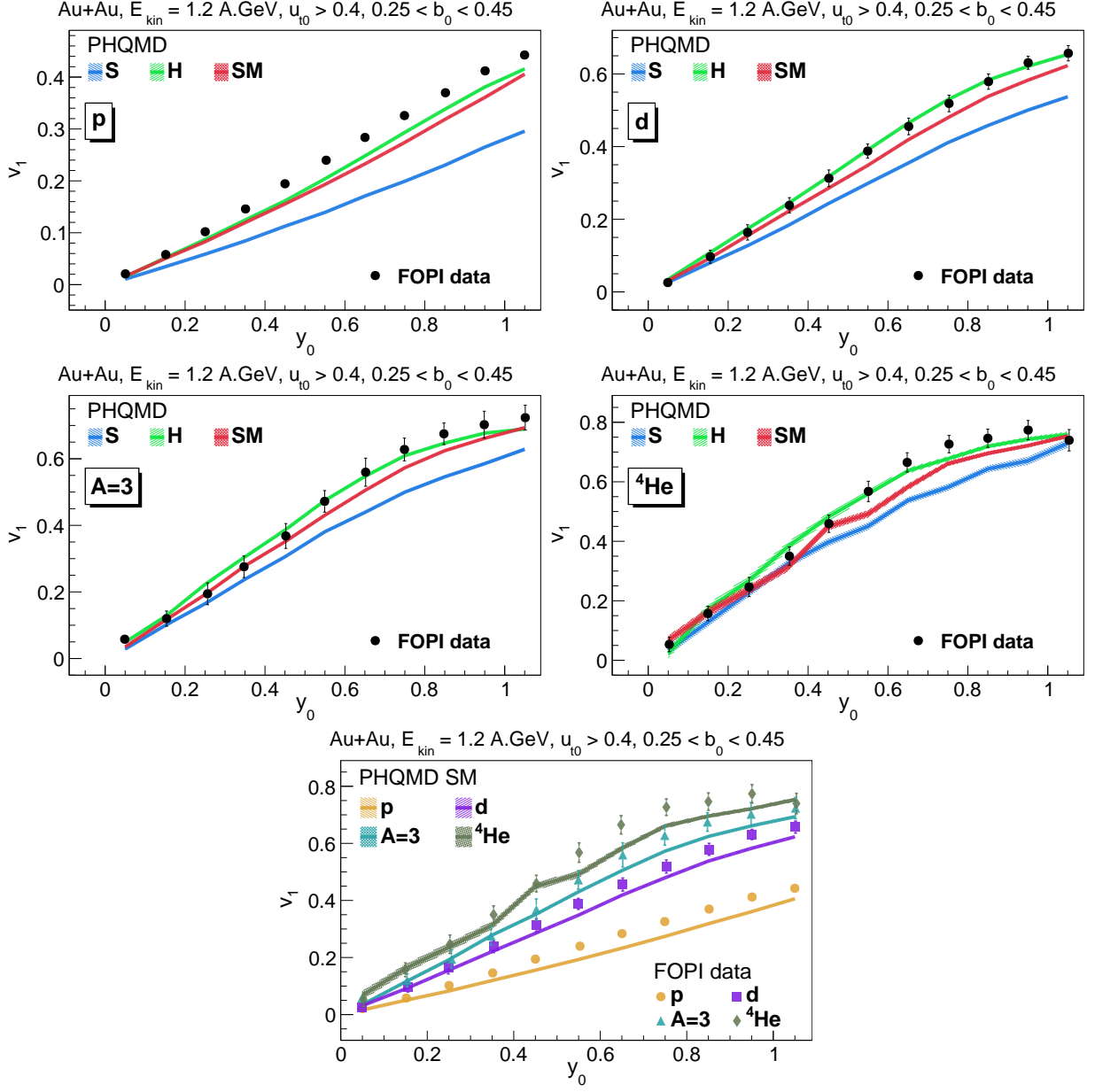


FIG. 13. v_1 of protons (upper left), deuterons (upper right), $A = 3$ (middle left) and ^4He (middle right) as a function of y_0 for Au+Au collisions at $E_{kin} = 1.2$ A GeV for $u_{t0} > 0.4$ and the impact parameter range $0.25 < b_0 < 0.45$. The blue line "S" corresponds to the PHQMD "soft" EoS, the green line "H" – to the "hard" EoS, the red line "SM" represents the momentum-dependent "soft" EoS. The plot on the lower row shows the compilation of $v_1(y_0)$ for protons, deuterons, $A = 3$ clusters and ^4He for the SM EoS. The FOPI experimental data are taken from Ref. [50].

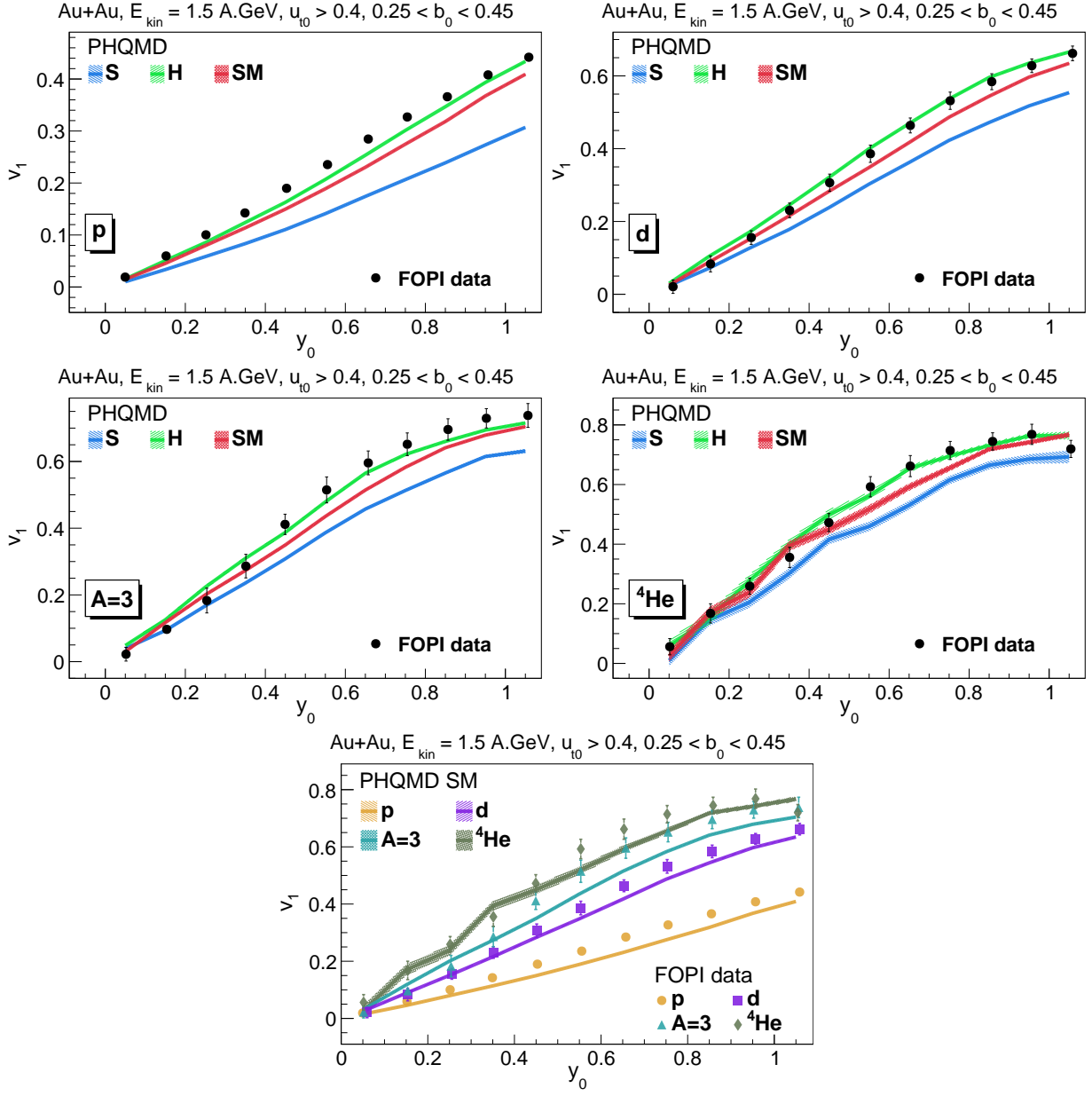


FIG. 14. v_1 of protons (upper left), deuterons (upper right), $A = 3$ (middle left) and ^4He (middle right) as a function of y_0 for Au+Au collisions at $E_{kin} = 1.5$ A GeV for $u_{t0} > 0.4$ and the impact parameter range $0.25 < b_0 < 0.45$. The blue line "S" corresponds to the PHQMD "soft" EoS, the green line "H" – to the "hard" EoS, the red line "SM" represents the momentum-dependent "soft" EoS. The plot on lower row shows the compilation of $v_1(y_0)$ for protons, deuterons, $A = 3$ clusters and ^4He for the SM EoS. The FOPI experimental data are taken from Ref. [50].

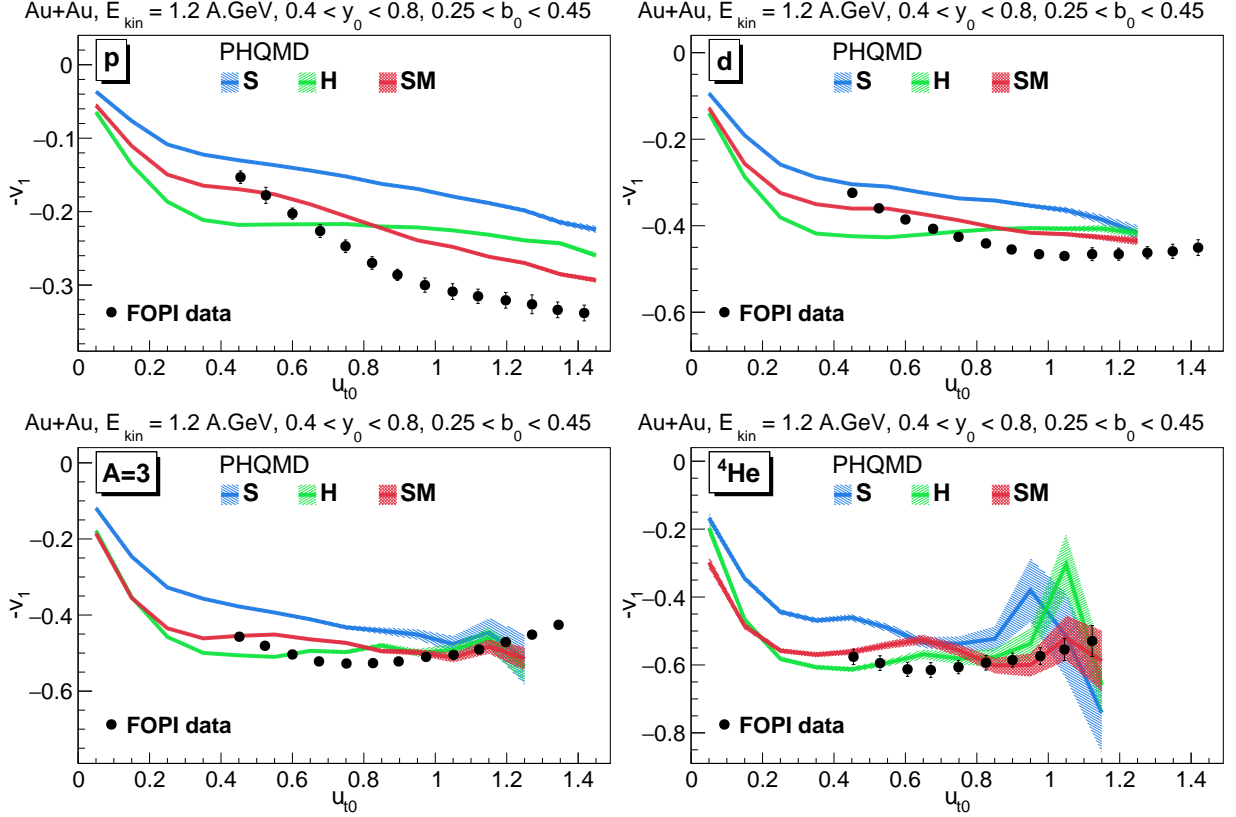


FIG. 15. v_1 of protons (upper left), deuterons (upper right), $A = 3$ (lower right) and ^4He (lower left) as a function of u_{t0} for Au+Au collisions at $E_{kin} = 1.2$ A GeV for $0.4 < y_0 < 0.8$ and the impact parameter range $0.25 < b_0 < 0.45$. The blue line "S" corresponds to the PHQMD "soft" EoS, the green line "H" – to the "hard" EoS, the red line "MS" represents the momentum-dependent "soft" EoS. The FOPI experimental data are taken from Ref. [50].

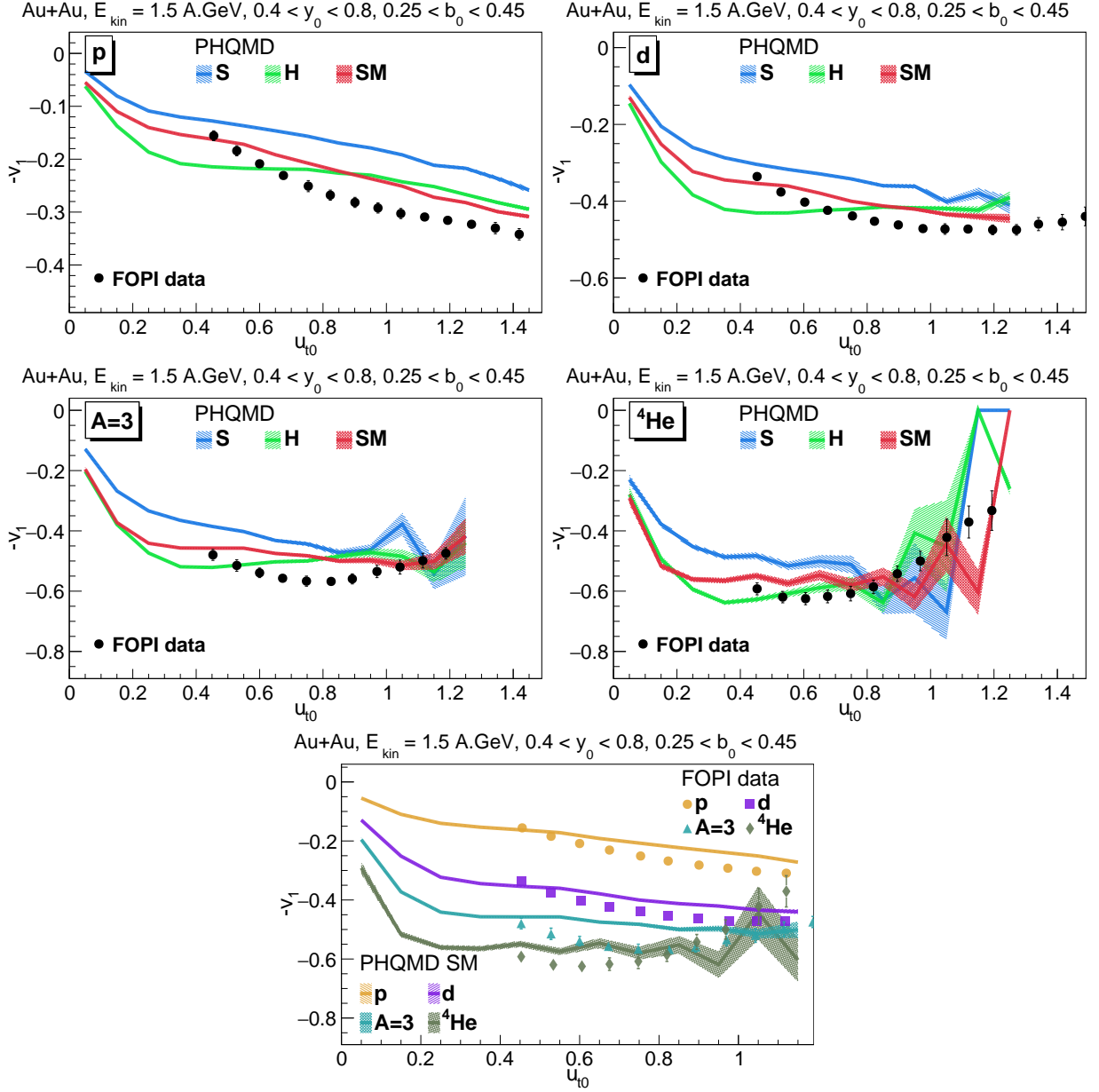


FIG. 16. v_1 of protons (upper left), deuterons (upper right), $A = 3$ (middle left) and ^4He (middle right) as a function of u_{t0} for Au+Au collisions at $E_{kin} = 1.5$ A.GeV for $0.4 < y_0 < 0.8$ and the impact parameter range $0.25 < b_0 < 0.45$. The blue line "S" corresponds to the PHQMD "soft" EoS, the green line "H" – to the "hard" EoS, the red line "SM" represents the momentum-dependent "soft" EoS. The plot on the lower row shows the compilation of $v_1(u_{t0})$ for protons, deuterons, $A = 3$ clusters and ^4He for the SM EoS. The FOPI experimental data are taken from Ref. [50].

C. The elliptic flow v_2

The second Fourier coefficient in the azimuthal distribution (24) - the elliptic flow v_2 - measures whether matter is preferably emitted in the reaction plane (positive v_2) or perpendicular to the reaction plane (negative v_2). At SIS energies, considered here, v_2 is negative. In former times this has been interpreted either as the absorption of participant nucleons by the spectator matter or as squeezing of the nucleons perpendicular to the reaction plane.

More detailed studies have revealed, however, that the origin of v_2 is more complicated [63] and that in reality 3 different processes contribute to the building of the v_2 [74]. Participant nucleons entering the spectator matter have to have a positive p_x component (if the spectator is located in positive x -direction). This positive p_x component gets lowered by finite angle collisions with spectator nucleons, creating an overall negative v_2 . In addition, nucleons sitting in y -direction at the tip of the overlap region, feel a very strong density gradient in y -direction (from about twice nuclear matter density to vacuum) and get therefore considerably accelerated in y -direction. This yields also a negative v_2 . Finally, the compressed matter of the overlap region, which is not spherical in transverse direction and approaches with increasing beam energy an almond shaped form, develops an outward non-isotropic pressure, which accelerates the participant nucleons outwards, preferably in x -direction due to the geometry. The v_2 is then an image of the initial eccentricity in coordinate space and is positive. This is the mechanism which dominates v_2 at higher energies but it is already present at the energies considered here. Collisions and potential interactions contribute both to v_2 and therefore it is a challenge for every transport approach to reproduce the experimentally observed v_2 values quantitatively.

1. Comparison of the PHQMD v_2 to the HADES data

The PHQMD results for $v_2(y)$ in comparison with the HADES data [49] are presented in Fig. 17 for protons for 20-30% central Au+Au collisions at $E_{kin}=1.23$ A GeV for different p_T intervals: $0.55 < p_T < 0.6$ GeV/c (upper), $0.75 < p_T < 0.8$ GeV/c (middle) and $0.95 < p_T < 1.0$ GeV/c (lower). We obtain, in agreement with the SMASH results [65], that a soft and a hard EoS cannot reproduce the observed proton elliptic flow, whereas the momentum-dependent interaction gives results which come close to the experimental HADES data [49], but still under-predict v_2 close to midrapidity independent of the p_T bin.

In Fig. 18 we show v_2 of protons (top left), deuterons (bottom left) and tritons (top right) as a function of rapidity for 20-30% central Au+Au collisions at $E_{kin} = 1.23$ A GeV for $1.0 < p_T < 1.5$ GeV/c in comparison to the HADES data [48]. The bottom right plot shows the

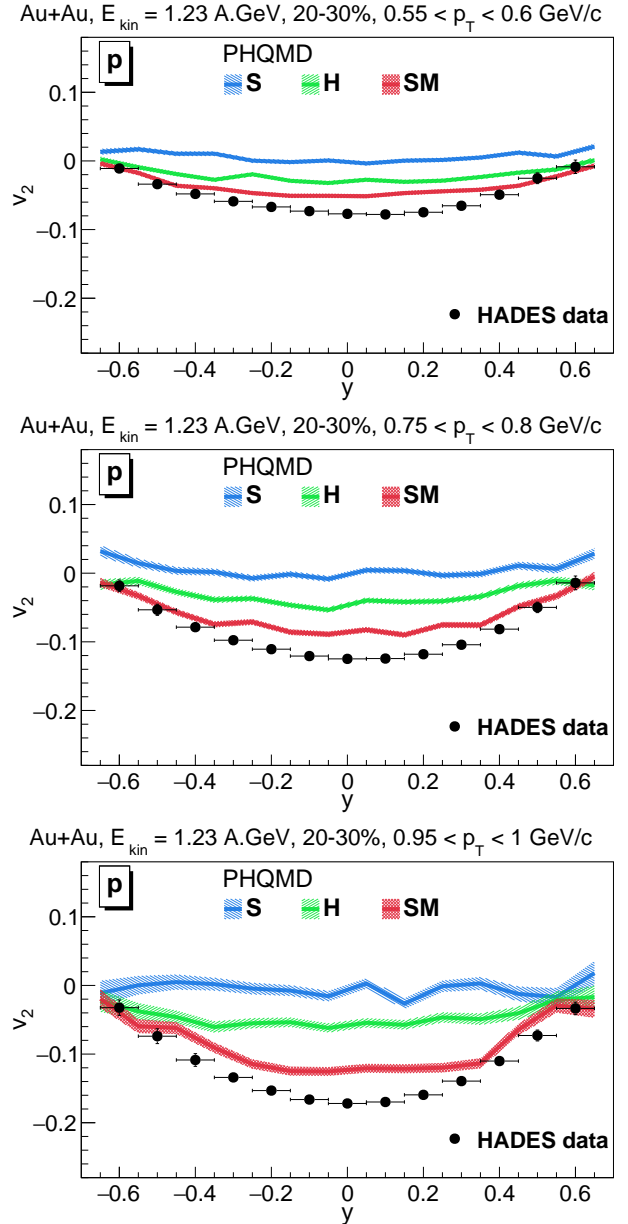


FIG. 17. v_2 of protons as a function of rapidity y for 20-30% central Au+Au collisions at $E_{kin} = 1.23$ A GeV for different p_T intervals: $0.55 < p_T < 0.6$ GeV/c (upper), $0.75 < p_T < 0.8$ GeV/c (middle) and $0.95 < p_T < 1.0$ GeV/c (lower). The blue lines "S" correspond to the PHQMD calculations with the "soft" EoS, the green lines "H" show the "hard" EoS, the red lines "SM" represent the momentum-dependent "soft" EoS. The HADES experimental data are taken from Ref. [49].

$v_2(y)$ of deuterons for the SM EoS produced by different mechanisms: kinetic (yellow line), MST (violet line) as well as the $v_1(y)$ of all deuterons (red line, identical to the SM result on the lower left plot). One can see that the $v_2(y)$ from kinetic and MST deuterons are rather similar (similar to $v_1(y)$ - cf. Fig. 10).

As seen from Fig. 18, the PHQMD results for protons,

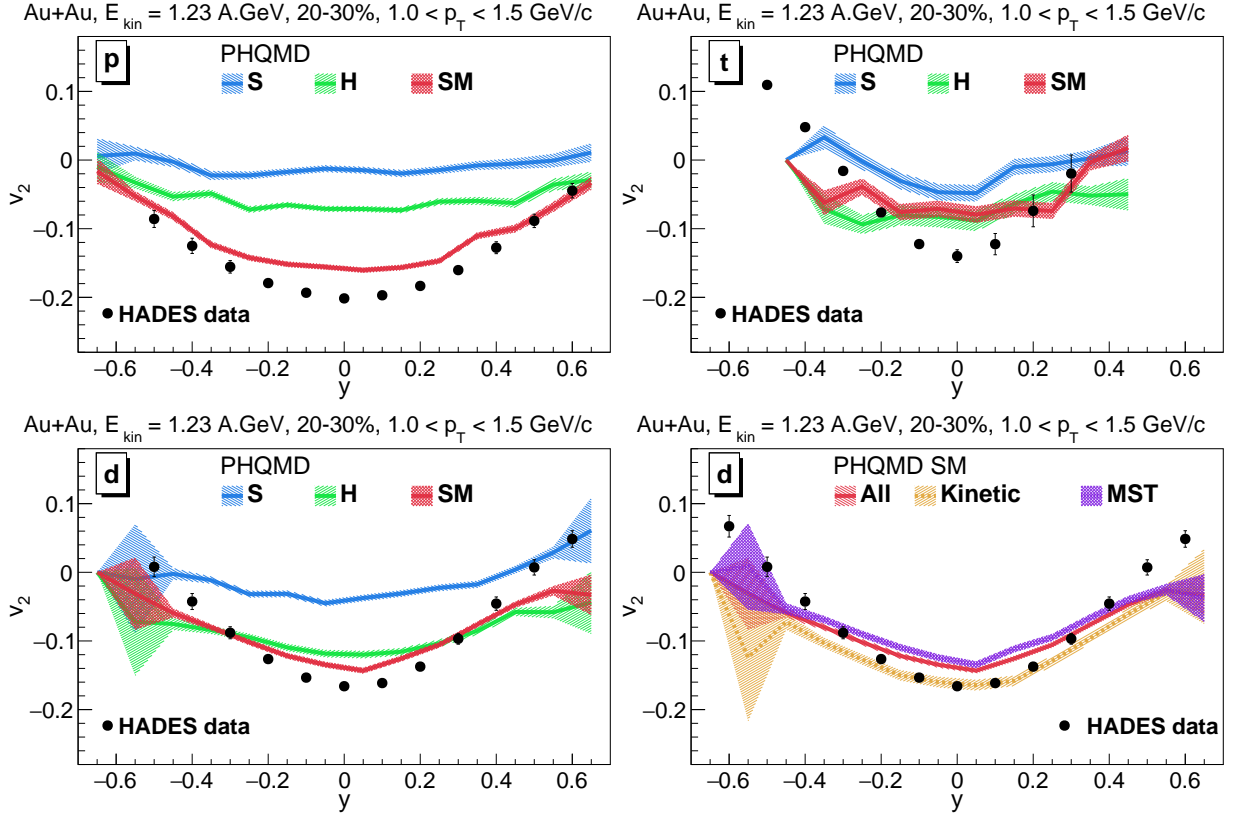


FIG. 18. v_2 of protons (upper left) and deuterons (lower row) and tritons (upper right) as a function of rapidity for 20-30% central Au+Au collisions at $E_{kin} = 1.23$ A GeV for $1.0 < p_T < 1.5$ GeV/c. The blue lines "S" correspond to the PHQMD calculations with the "soft" EoS, the green lines "H" show the "hard" EoS, the red lines "SM" represent the momentum-dependent "soft" EoS. The low right plot shows the $v_2(y)$ of deuterons for the SM EoS produced by different mechanisms: kinetic (yellow line), MST (violet line) as well as the $v_1(y)$ of all deuterons (red line, identical to the SM result on the lower left plot). The HADES experimental data are taken from Ref. [48].

deuterons and tritons with the soft EoS substantially underestimate $v_2(y)$ at this interval of large p_T . The hard EoS leads to an underestimation of the proton v_2 (similar to the results in Fig. 17 for the intervals of smaller p_T , while the SM EoS gives a good description of the HADES data for the proton v_2 , deuterons and tritons which agree within 10% with the experimental data. For the latter two $v_2(y)$ are rather similar for the SM and hard EoS. This result agrees with the UrQMD calculations with a hard EoS in Ref. [26], but in tension with the SMASH results [65], where a hard EoS gives a larger v_2 than observed experimentally. We note that in these calculations deuterons are determined by coalescence.

The transverse momentum distribution of v_2 is presented in Fig. 19 for protons (top), deuterons (middle) and tritons (bottom) as a function of p_T for rapidity intervals $|y| < 0.05$ (left column) and $-0.45 < y < -0.35$ (right column) for 20-30% central Au+Au collisions at $E_{kin}=1.23$ A GeV. First of all we observe a strong p_T dependence of $v_2(p_T)$ and a strong dependence on EoS for all clusters and both rapidity intervals. For both rapidity intervals the soft EoS leads to a substantial underestimation of the HADES data on $v_2(p_T)$ for protons, deuterons and tritons and the deviation grows with increasing p_T . For the hard EoS the HADES data of the proton v_2 at high p_T are not reproduced, what is in line with SMASH results [65]. The soft momentum-dependent EoS brings, however, v_2 close to the experimental data. Whereas for protons $v_2(p_T)$ is different for a H and a SM EoS, for deuterons and tritons they yield almost the same result, at forward as well as at mid rapidity. A hard EoS gives deuterons more v_2 than protons and brings the calculations closer to the experimental data. This has also been observed in UrQMD calculations in Ref. [26]. It is interesting to note that the functional form of the experimental $v_2(p_T)$ for protons, deuterons and tritons is different, especially for in $-0.45 < y < -0.35$ interval. The PHQMD calculations reproduce qualitatively the forms as well as the values of measured $v_2(p_T)$.

Fig. 20 presents the elliptic flow scaled by the atomic number - v_2/A as a function of the transverse momentum of a nucleon in the cluster p_T/A for protons, deuterons and tritons at midrapidity $|y| < 0.05$. The scaled $v_2/A(p_T/A)$ is almost independent of A .

This scaling behavior of $v_2/A(p_T/A)$ has been observed by the HADES collaboration [49, 75]. For the deuterons or tritons this means that their azimuthal distribution can be obtained by assuming that two nucleons, with an azimuthal distribution as seen for the protons, combine to a deuteron and, correspondingly, to larger clusters. We note that a similar scaling behavior of v_2 with the number of "constituents" has been predicted in Ref. [76] for the v_2 of mesons and baryons with the number of valence quarks (i.e. 2 for mesons and 3 for baryons). This 'constituent quark number scaling' has been observed experimentally in central Au+Au collisions at RHIC [77, 78].

As follows from Fig. 20, the PHQMD calculations show that in this scaled presentation of v_2 the difference

between the $v_2(p_T)$ distributions for protons and clusters is reduced substantially but we do not observe a perfect scaling, as the data show for $p_T < 0.8$ GeV/c (we note also that we have a limited statistics in our simulations). Our v_2 for the SM EoS is also lower than that observed experimentally - in line with Fig. 19.

2. Comparison of the PHQMD v_2 to the FOPI data

We step now to a comparison of the PHQMD results with the experimental data from the FOPI Collaboration [50]. To allow for a better comparison with the HADES data we have changed the representation of v_2 from the FOPI Collaboration by plotting v_2 instead of $-v_2$, as done in Ref. [50]. In Figs. 21 and 22 we show the elliptic flow (v_2) of protons, deuterons and ${}^4\text{He}$ as a function of the scaled rapidity y_0 for Au+Au collisions at $E_{kin}=1.2$ and 1.5 A GeV for $u_{t0} > 0.4$ and the impact parameter range $0.25 < b_0 < 0.45$ for three EoS. One can see that for the both energies the v_2 of protons is underestimated for all 3 EoS in the considered u_{t0} interval, as was the case for the HADES data. The SM EoS gives the largest v_2 , followed by the hard EoS. The lowest elliptic flow comes from the soft EoS. For deuterons and tritons the hard EoS gives slightly larger v_2 values than the SM EoS while the soft EoS gives the lowest contribution. The deuterons are best described by a H EoS whereas the triton data are very close to a SM EoS.

In the lower right plot of Fig. 22 we compile of $v_2(y_0)$ the experimental results and the theoretical prediction with a SM EoS for protons, deuterons, $A = 3$ clusters and ${}^4\text{He}$. This shows that the rapidity distributions of v_2 for the different cluster differ significantly. This is qualitatively reproduced by the PHQMD calculations, for the clusters even better than for the free protons.

As already stated, the $v_2(y_0)$ coefficients for the FOPI data in Figs. 21 and 22 are shown for the selected interval of u_{t0} . The results for $v_2(y_0)$ for $u_{t0} > 0.4$ can be better understood if one studies the u_{t0} dependence of the flow explicitly.

The experimental and the PHQMD results for $v_2(u_{t0})$ at midrapidity, $|y_0| < 0.4$, are shown in Figs. 23 and 24. These figures show the v_2 of protons, deuterons, tritons and ${}^4\text{He}$ as a function of the scaled transverse momentum u_{t0} for the $0.25 < b_0 < 0.45$ impact parameter range for Au+Au collisions at $E_{kin}=1.2$ and 1.5 A GeV, respectively. One can see that for protons the v_2 dependence on u_{t0} , as predicted by PHQMD, is much stronger than that for the experimental data, an observation which is a bit surprising in view of the fact that for the HADES data the p_T dependence of v_2 is reasonably well described by PHQMD calculations with a SM EoS. This explains the mismatch of $v_2(y_0)$ between theory and experiment in Figs. 21 and 22, where the lower u_{t0} boundary is 0.4. The deviation is stronger for large u_{t0} , i.e. for the region which is selected for Figs. 21 and 22. The v_2 dependence on u_{t0} of the experimental data for deuterons and

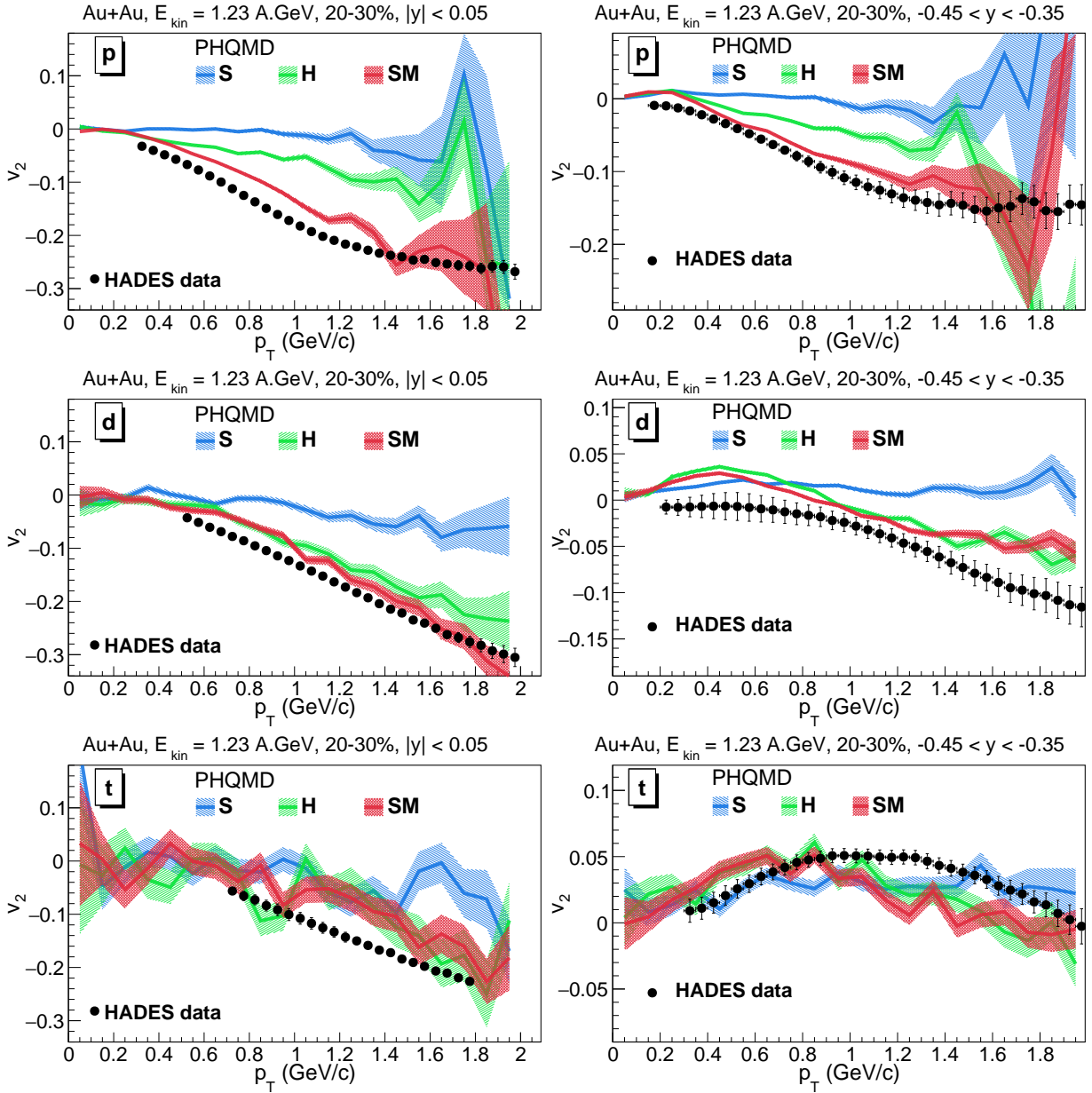


FIG. 19. v_2 of protons (upper row), deuterons (middle row) and triton (lower row) as a function of p_T for rapidity intervals $|y| < 0.05$ (left column) and $-0.45 < y < -0.35$ (right column) for 20-30% central Au+Au collisions at $E_{kin}=1.23$ A GeV. The blue lines "S" correspond to the PHQMD calculations with the "soft" EoS, the green lines "H" show the "hard" EoS, the red lines "SM" represent the momentum-dependent "soft" EoS. The HADES experimental data are taken from Ref. [48, 49].

tritons is well described by PHQMD employing a hard EoS, which results in slightly larger values of v_2 than the SM EoS, while the soft EoS underestimates clearly v_2 for protons and clusters.

The plot on the lower row of Fig. 23 shows the compilation of $v_2(u_{t0})$ for protons, deuterons, tritons and ${}^4\text{He}$ for the SM EoS at $E_{kin}=1.2$ A GeV in comparison with the experimental data. Also the FOPI data show a nontrivial dependence of the slope on the mass of the clusters. The difference between protons and clusters is substantially reduced if one displays v_2/A instead of v_2 as one can see

from the bottom right panel of this figure. We see for the FOPI data now an almost perfect scaling of the calculation for $u_{t0} < 0.8$ in the PHQMD calculation (which is also present if we replace u_{t0} by p_T), whereas the data do not show such a scaling. In Fig. 24 we display only the compilation because the error bars are too large for that a scaling presentation is meaningful.

Comparing the PHQMD calculations with the data sets from HADES and FOPI one can conclude that overall the PHQMD calculations describe qualitatively the features of the data. For both data sets we observe, us-

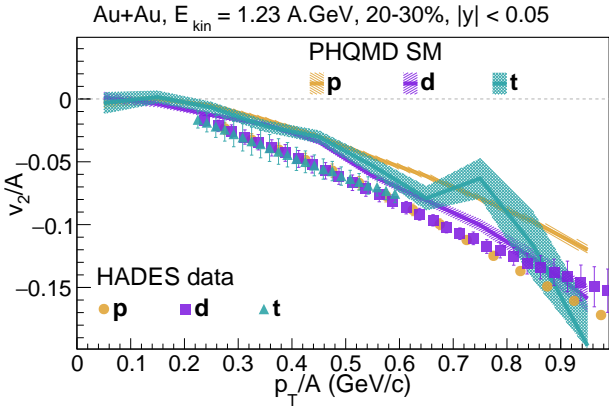


FIG. 20. The elliptic flow scaled with atomic number v_2/A versus scaled p_T/A for protons, deuterons and tritons for 20-30% central Au+Au collisions for $|y| < 0.05$ at $E_{kin}=1.23$ A GeV. The HADES experimental data are taken from Ref. [48] and scaled with A .

ing a SM EoS, a slight underestimation of the slope of $v_1(y)$ for protons as well as clusters. For the $v_1(p_T)$ the situation is more complex. For the HADES data the SM calculation underestimates slightly the $v_1(p_t)$ at high p_T but reproduces the functional form whereas the PHQMD calculation with a SM EoS agree with the FOPI v_1 data for $A = 3$ and 4He at large u_{t0} but miss the functional form of $v_1(u_{t0})$.

For $v_2(y)$ the functional form of the data is similar in all three data sets and reproduced qualitatively as well by PHQMD calculations, best for a SM EoS which underestimates nevertheless the v_2 , especially at midrapidity. The PHQMD calculations for the three data sets, i.e. for Au+Au for 1.23 A GeV from the HADES Collaboration and for 1.2 and 1.5 A GeV from the FOPI Collaboration, show a similar functional form. Please note, that the HADES and FOPI data presented here are for different centrality ranges. While the HADES data is measured for 20-30% most central events, the FOPI event selection is for the impact parameter range $0.25 < b_0 < 0.45$, roughly corresponding to the 6-20% most central events. Differences in the quality of agreement between PHQMD calculations and data might therefore to some extent be attributed to the different methods of centrality definition, which should be modeled in a more detailed fashion in the future.

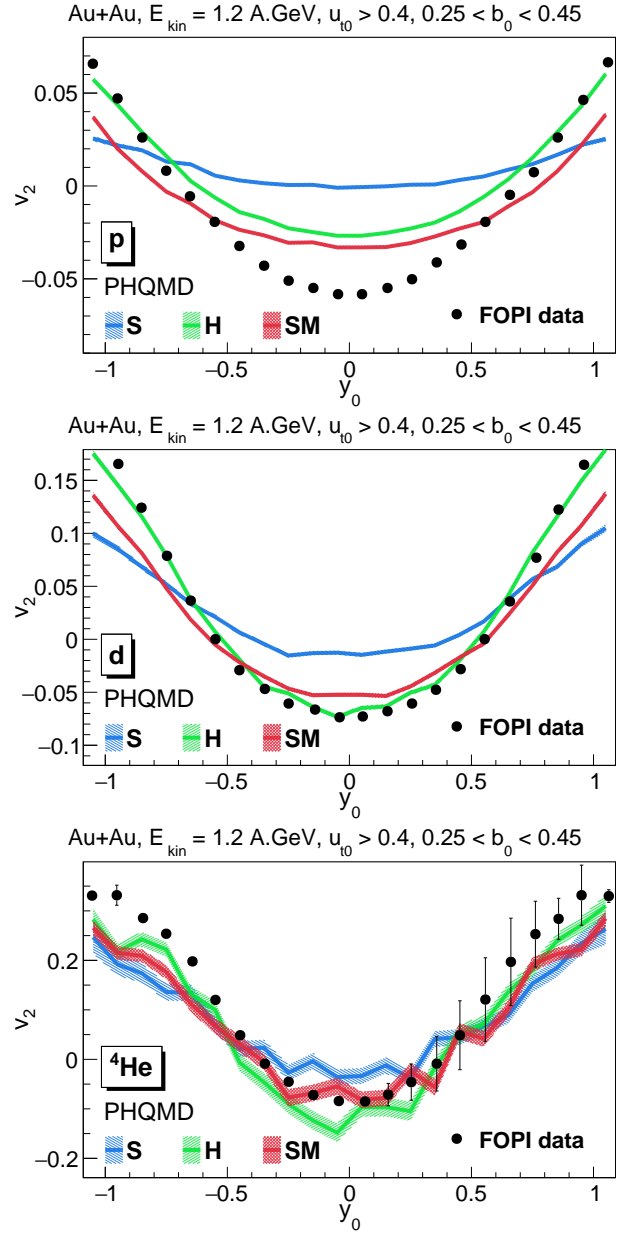


FIG. 21. v_2 of protons (upper), deuterons (middle) and 4He (lower) as a function of the scaled rapidity y_0 for Au+Au collisions at $E_{kin}=1.2$ A GeV for $u_{t0} > 0.4$ and the impact parameter range $0.25 < b_0 < 0.45$. The blue lines "S" correspond to the PHQMD calculations with the "soft" EoS, the green lines "H" show the "hard" EoS, the red lines "SM" represent the momentum-dependent "soft" EoS. The FOPI experimental data are taken from Ref. [50].

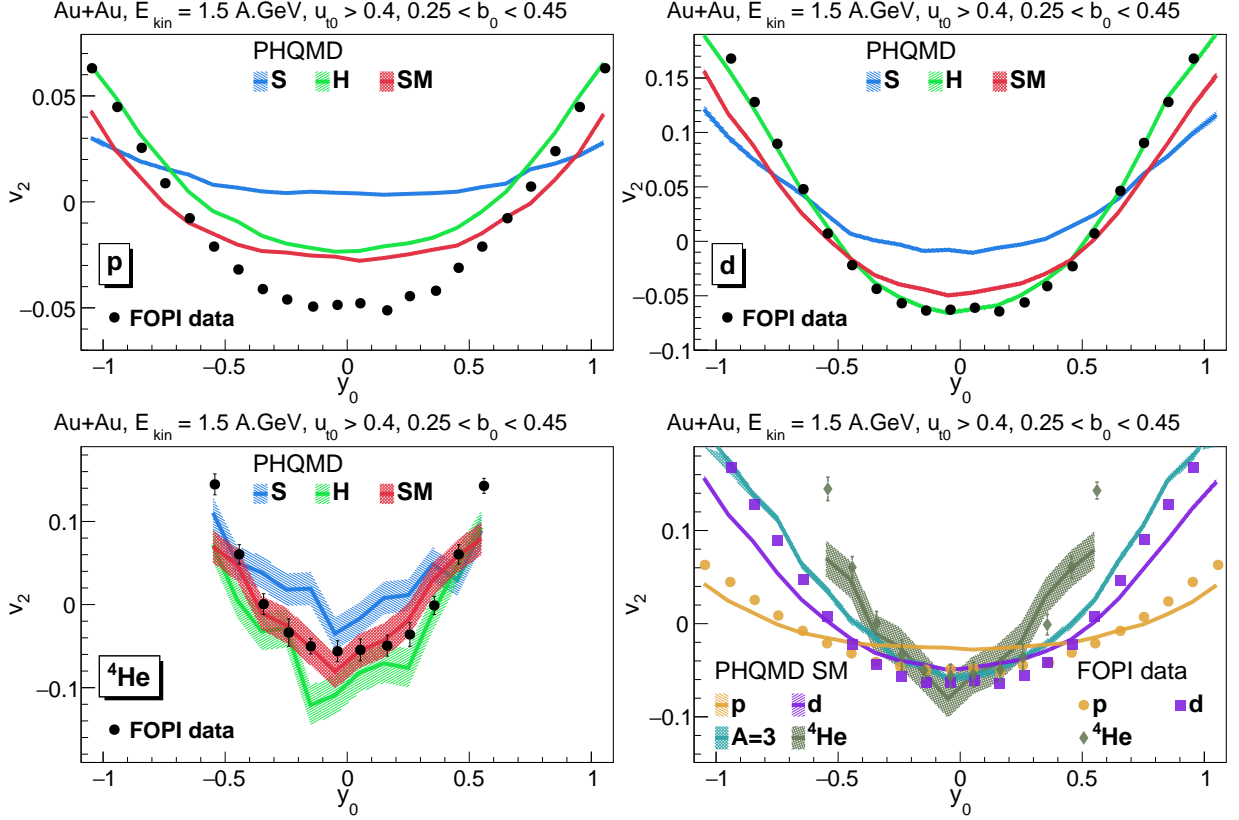


FIG. 22. v_2 of protons (upper left), deuterons (upper right) and ^4He (lower left) as a function of the scaled rapidity y_0 for Au+Au collisions at $E_{kin}=1.5$ A GeV for $u_{t0} > 0.4$ and the impact parameter range $0.25 < b_0 < 0.45$. The blue lines "S" correspond to the PHQMD calculations with the "soft" EoS, the green lines "H" show the "hard" EoS, the red lines "SM" represent the momentum-dependent "soft" EoS. The lower right plot shows the compilation of $v_2(y_0)$ for protons, deuterons, $A = 3$ clusters and ^4He for the SM EoS. The FOPI experimental data are taken from Ref. [50].

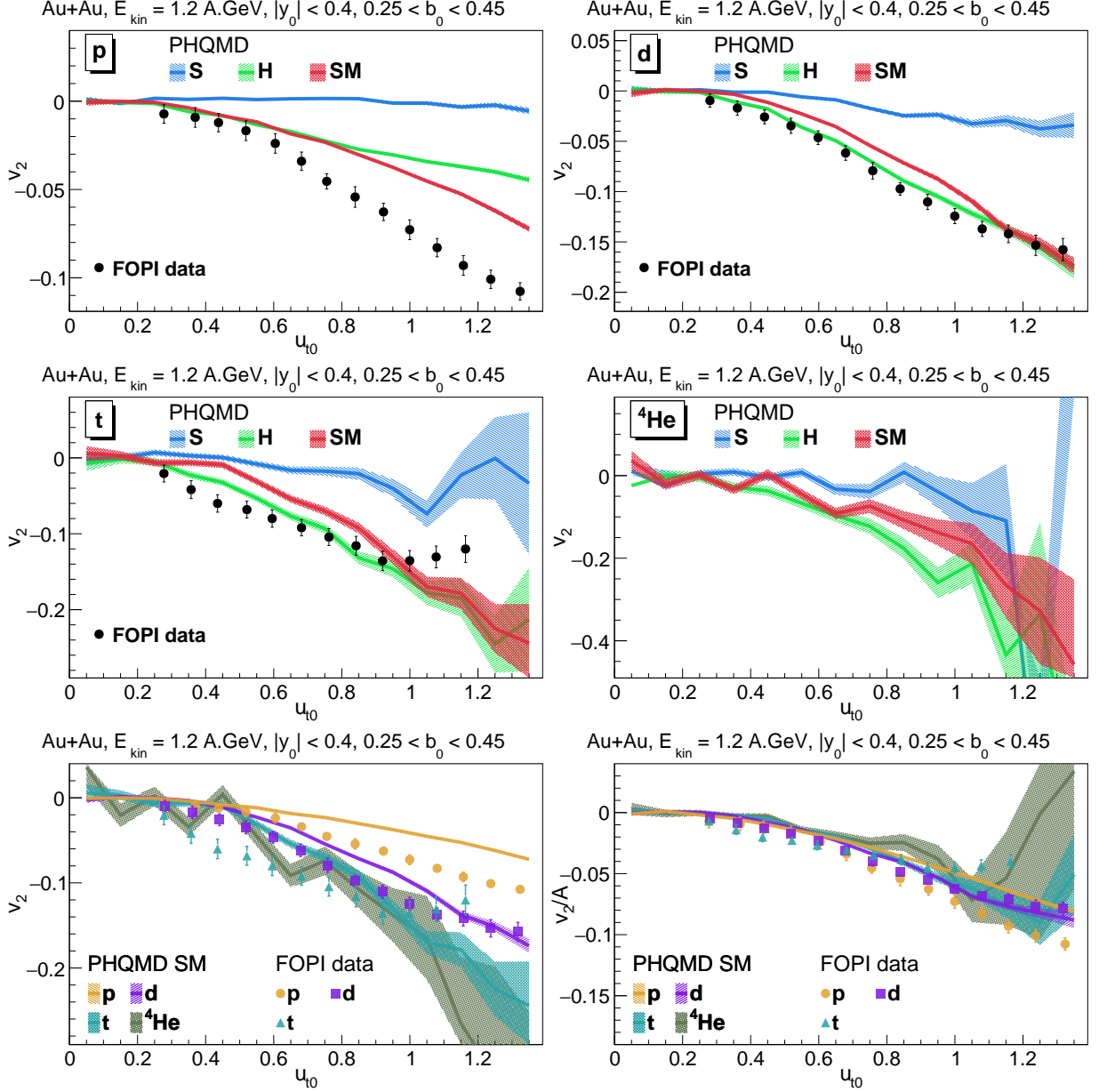


FIG. 23. v_2 of protons (upper left), deuterons (upper right), tritons (middle left) and ^4He (middle right) as a function of scaled transverse momentum u_{t0} for $|y_0| < 0.4$ and the $0.25 < b_0 < 0.45$ impact parameter range for Au+Au collisions at $E_{kin} = 1.2$ A GeV. The blue lines "S" correspond to the PHQMD calculations with the "soft" EoS, the green lines "H" show the "hard" EoS, the red lines "SM" represent the momentum-dependent "soft" EoS. The left plot in the lower row shows the compilation of $v_2(u_{t0})$ for protons, deuterons, tritons and ^4He for the SM EoS; the right plot shows the scaled $v_2/A(u_{t0})$. The FOCI experimental data are taken from Ref. [50].

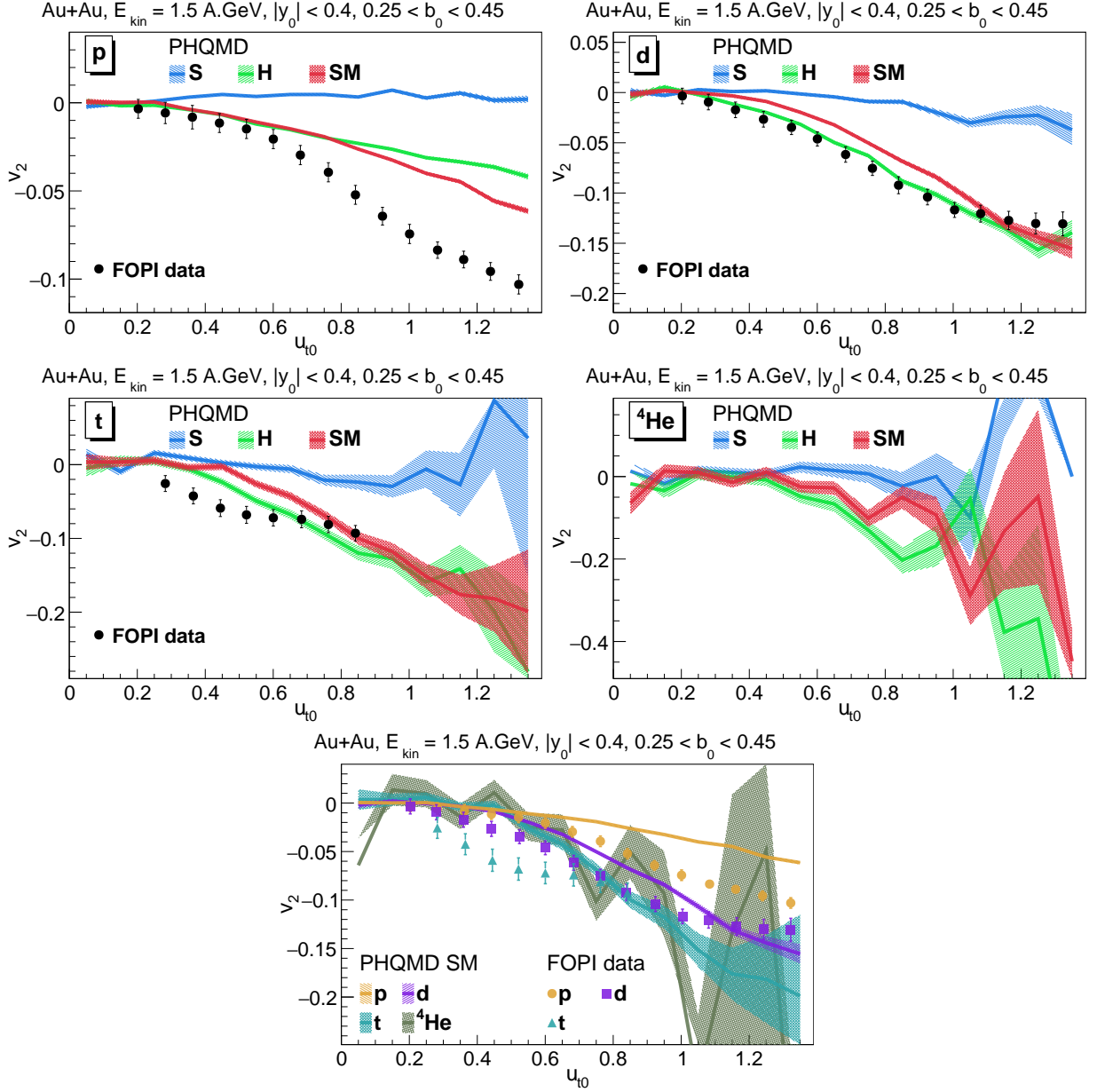


FIG. 24. v_2 of protons (upper left), deuterons (upper right), tritons (middle left) and ^4He (middle right) as a function of scaled transverse momentum u_{t0} for $|y_0| < 0.4$ and the $0.25 < b_0 < 0.45$ impact parameter range for Au+Au collisions at $E_{kin}=1.5$ A GeV. The blue lines "S" correspond to the PHQMD calculations with the "soft" EoS, the green lines "H" show the "hard" EoS, the red lines "SM" represent the momentum-dependent "soft" EoS. The plot on the lower row shows the compilation of $v_2(u_{t0})$ for protons, deuterons, tritons and ^4He for the SM EoS. The FOCI experimental data are taken from Ref. [50].

V. SENSITIVITY OF v_1 AND v_2 OF DEUTERONS ON THE PRODUCTION MECHANISM: MST + KINETIC VERSUS COALESCENCE

In this section we investigate the sensitivity of the flow observables v_1 and v_2 to the deuteron production mechanisms. For that goal we compare the PHQMD results for the "default" scenario, where deuterons are produced by the kinetic + MST mechanisms, to the coalescence mechanism. We stress that the PHQMD is a unique laboratory for such a comparison since all scenarios are integrated in the same code and applied to the same events.

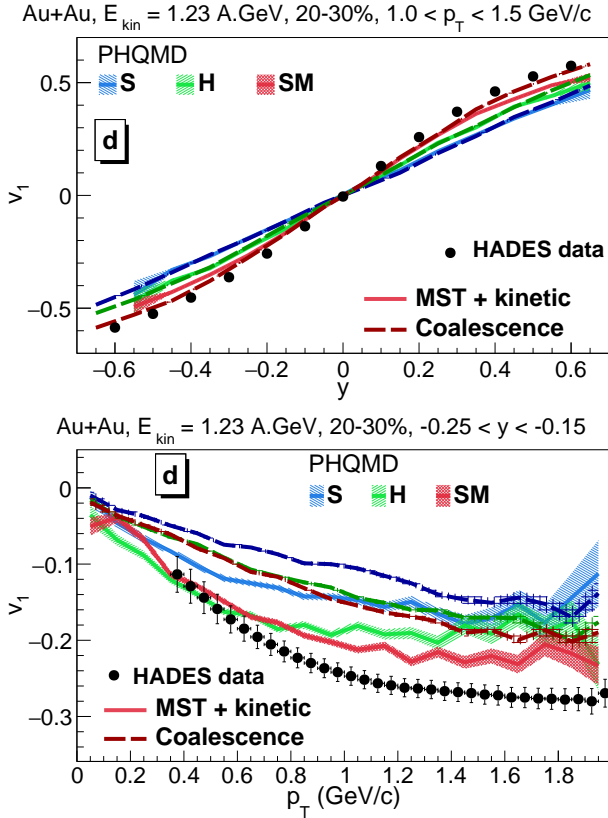


FIG. 25. Upper plot: Comparison of the $v_1(y)$ of deuterons produced by kinetic + MST mechanisms (solid lines) with the coalescence mechanism (dashed lines) for 20-30% central Au+Au collisions at $E_{kin} = 1.23$ A GeV for $1.0 < p_T < 1.5$ GeV/c. Lower plot: The comparison of $v_1(p_T)$ of deuterons produced by kinetic + MST mechanisms (solid lines) with the coalescence mechanism (dashed lines) for 20-30% central Au+Au collisions for $-0.25 < y < -0.15$. The blue lines "S" correspond to the PHQMD calculations with the "soft" EoS, the green lines "H" show the "hard" EoS, the red lines "SM" represent the momentum-dependent "soft" EoS. The color coding for the coalescence results is the same but in dark colors. The HADES experimental data are taken from Ref. [48].

In the upper plot of Fig. 25 we present the comparison of $v_1(y)$ of deuterons produced by the "default" scenario

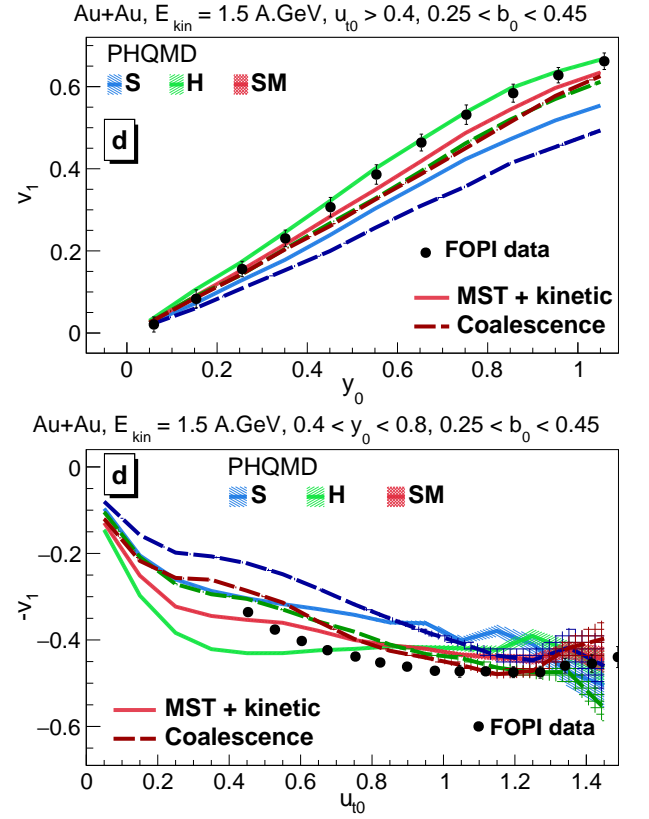


FIG. 26. Upper plot: Comparison of the $v_1(y_0)$ of deuterons (upper right) produced by kinetic + MST mechanisms (solid lines) with the coalescence mechanism (dashed lines) for Au+Au collisions at $E_{kin} = 1.5$ A GeV for $u_{t0} > 0.4$ and the impact parameter range $0.25 < b_0 < 0.45$. Lower plot: Comparison of $v_1(u_{t0})$ of deuterons produced by kinetic + MST mechanisms (solid lines) with the coalescence mechanism (dashed lines) for Au+Au collisions at $E_{kin} = 1.5$ A GeV for $0.4 < y_0 < 0.8$ and centrality $0.25 < b_0 < 0.45$. The color coding is the same as in Fig. 25. The FOPI experimental data are taken from Ref. [50].

in PHQMD - kinetic + MST mechanisms (solid lines, as shown in Figs. 10 and 12, respectively) to the coalescence mechanisms (dashed lines in dark colors) for 20-30% central Au+Au collisions at $E_{kin} = 1.23$ A GeV for $1.0 < p_T < 1.5$ GeV/c. The lower plot of Fig. 25 shows a similar comparison for $v_1(p_T)$ for the rapidity interval $-0.25 < y < -0.15$. Both deuteron production scenarios are confronted with the HADES data [48]. One can see that the v_1 of kinetic + MST deuterons is slightly larger than those from coalescence for all EoS, which is in line with our findings in Ref. [47] that the nucleons, identified as being a part of deuterons by coalescence and by MST, are only partially identical.

Figure 26 shows - similar to Fig. 25 - a comparison of $v_1(y_0)$ and $v_1(u_{t0})$, but with respect to the FOPI data [50]. The results for the kinetic + MST mechanisms are the same as in Figs. 14 and 16, respectively.

The upper plot of Fig. 27 displays the comparison of

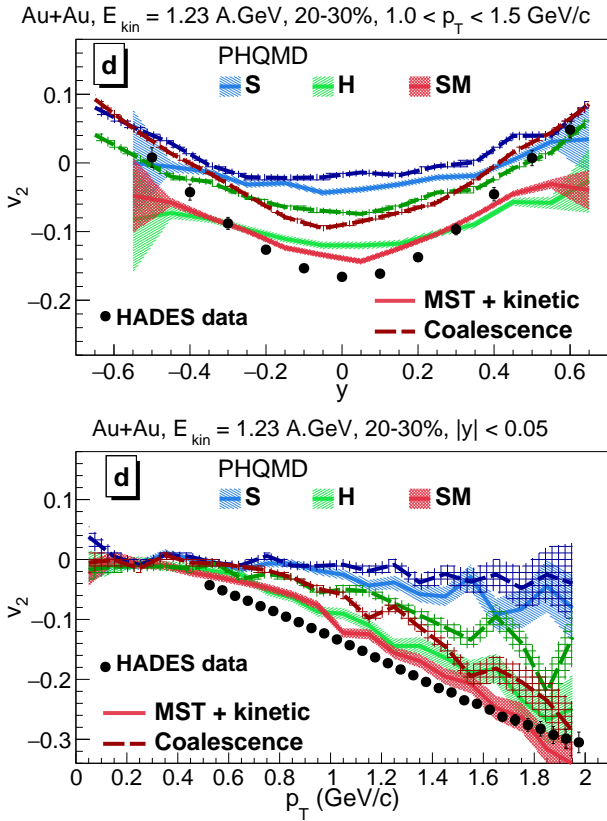


FIG. 27. Upper plot: Comparison of $v_2(y)$ of deuterons produced by kinetic + MST mechanisms (solid lines) with the coalescence mechanism (dashed lines) for 20-30% central Au+Au collisions at $E_{kin} = 1.23$ A GeV for $1.0 < p_T < 1.5$ GeV/c. Lower plot: Comparison of $v_2(p_T)$ of deuterons produced by kinetic + MST mechanisms (solid lines) with the coalescence mechanism (dashed lines) for 20-30% central Au+Au collisions for $|y| < 0.05$. The color coding is the same as in Fig. 25. The HADES experimental data are taken from Ref. [48].

$v_2(y)$ of deuterons produced by kinetic + MST mechanisms (solid lines) to the coalescence mechanism (dashed lines) for 20-30% central Au+Au collisions at $E_{kin} = 1.23$ A GeV for $1.0 < p_T < 1.5$ GeV/c. The lower plot of Fig. 27 shows a similar comparison for $v_2(p_T)$ for rapidity interval $|y| < 0.05$. The both deuteron production scenarios are confronted with the HADES data [48]. The results for the kinetic + MST mechanisms are the same as in Figs. 18 and 19, respectively.

Figure 28 shows - similar to Fig. 27 - comparison of $v_2(y_0)$ and $v_2(u_{t0})$ but with respect to the FOPI data [50] for Au+Au collisions at $E_{kin} = 1.5$ A GeV for $u_{t0} > 0.4$ and the impact parameter range $0.25 < b_0 < 0.45$. The results for the kinetic + MST mechanisms are the same as in Figs. 22 and 24, respectively.

We find a substantial difference in the flow results on v_1 and v_2 obtained with the standard PHQMD calculations, which include kinetic and MST deuterons, to those obtained with the coalescence mechanism as used in the

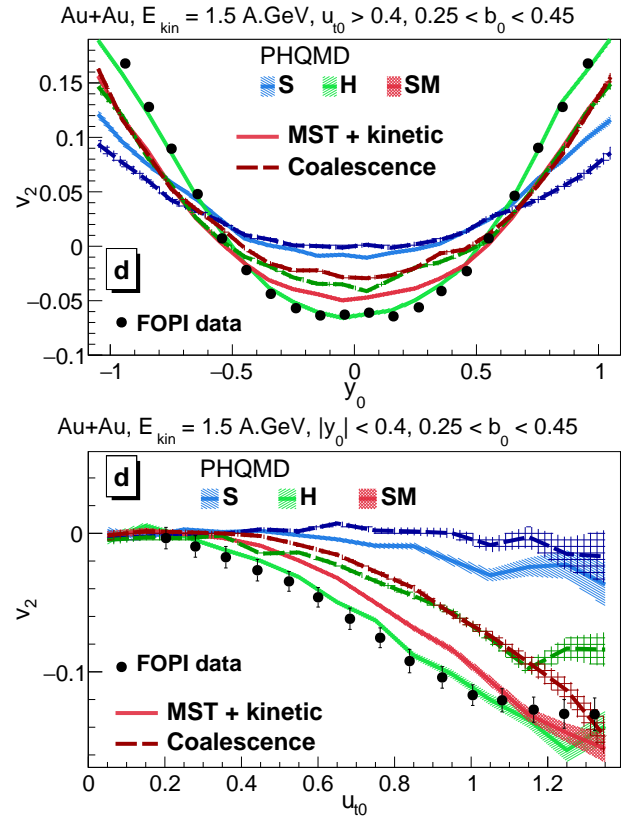


FIG. 28. Upper plot: Comparison of $v_2(y_0)$ of deuterons (upper right) produced by kinetic + MST mechanisms (solid lines) with the coalescence mechanism (dashed lines) for Au+Au collisions at $E_{kin} = 1.5$ A GeV for $u_{t0} > 0.4$ and the impact parameter range $0.25 < b_0 < 0.45$. Lower plot: The comparison of $v_2(u_{t0})$ of deuterons produced by kinetic + MST mechanisms (solid lines) with the coalescence mechanism (dashed lines) for Au+Au collisions at $E_{kin} = 1.5$ A GeV for $|y_0| < 0.4$ and centrality $0.25 < b_0 < 0.45$. The color coding is the same as in Fig. 25. The FOPI experimental data are taken from Ref. [50].

UrQMD and SMASH models. This observation demonstrates that the flow coefficients v_1 and v_2 are very sensitive to the production mechanisms (calculated within the same model) and can complement the information which can be derived from dN/dy and p_T distributions [47], both of which can help to identify experimentally the origin of the deuteron production in heavy-ion collisions.

VI. SUMMARY

In this study we have investigated the sensitivity of the directed flow v_1 and elliptic flow v_2 of protons and light clusters on the EoS at SIS energies. Our study is based on the PHQMD microscopic transport approach which has been extended by implementing a momentum-dependent interaction in terms of a potential. This allows us to study three EoS, i.e. a soft (S), hard (H) and soft momentum-dependent (SM) EoS, where the S and SM potentials share the same compressibility modulus of $K = 200$ MeV (defined for the infinite strongly interacting matter), while the hard EoS has a compressibility modulus of $K = 380$ MeV.

Our findings are summarized as follows:

- The PHQMD calculations confirm the earlier findings that the equation-of-state has a strong influence on the rapidity and on the transverse momentum-dependence of v_1 and v_2 of protons and light clusters created in heavy-ion collisions at SIS energies.
- The momentum-dependence of the equation-of-state, realized via a momentum-dependent potential acting between baryons, has a strong influence on v_1 and v_2 of protons and clusters. A soft momentum-dependent interaction yields v_1 and v_2 values which are close to that obtained for a hard EoS and quite different from those obtained with a static soft EoS, despite of the fact that the soft and soft momentum-dependent potentials share the same compressibility (cf. Table 1) for cold nuclear matter, whereas that of a hard EoS is much larger. Because we know from elastic pA collision that the nucleon-nucleon potential is momentum-dependent, the theoretical analysis of the flow coefficients with only static nucleon-nucleon potentials leads to misleading conclusions of the compressibility of nuclear matter.
- The comparison of the PHQMD calculations with a S, H and SM equation-of-state shows that the best description of the experimental proton data on v_1, v_2 at SIS energies, i.e. for Au+Au at $E_{kin}=1.23$ A GeV measured by the HADES collaboration as well as for Au+Au at $E_{kin}=1.2$ A GeV and 1.5 A GeV measured by the FOPI collaboration, is obtained by calculations with the soft momentum-dependent interaction. For light clusters calculations with a SM and a H EoS provide quite similar results. The soft static EOS with a compression modulus of $K = 200$ MeV is not supported by the considered three sets of experimental data.
- The PHQMD results with a SM EoS slightly underpredicts the measured v_1 and v_2 values, so the experimental data suggest that the compressibility of a SM equation-of-state, used in our calculations, is

slightly too low. A Bayesian analysis may help to fix the compressibility which describes best the set of data.

- $v_1(y)$ and $v_2(y)$, as well as $v_1(p_T)$ and $v_2(p_T)$, of light cluster are rather different from that of protons, in the experiments as well as in PHQMD calculations, which qualitatively reproduce the data. At midrapidity we find that v_1/A and v_2/A scale as a function of p_T/A confirming the experimental findings.
- The flow data are therefore a tool to study in which phase space regions clusters are produced during the heavy-ion collision.
- Deuterons determined by MST+kinetic have other v_1 and v_2 coefficients than that produced by coalescence. The difference is sufficiently large that it may help to identify the cluster production mechanism realized in nature.

The PHQMD calculations (as well as recent calculations by SMASH and UrQMD) reproduce the functional form of the experimental data and come also quantitatively close to the experimental results. This is a great achievement of transport approaches because especially v_2 is an observable which depends in a sensitive way on many features of these models, i.e. the potential, the realization of collisions as well as the initial distributions of the projectile and target nucleons in coordinate and momentum space.

To make further progress for the determination of the equation-of-state a better agreement of the event selection in theory and experiment has to be achieved, i.e. the impact parameter cuts have to be replaced by a centrality determination in line with experimental acceptance and procedure. Also the systematic error for v_1 and v_2 in the different theoretical approaches has to be established, which includes the uncertainties due to the different numerical set-ups as well as due to the different implementations of the momentum-dependent potential in mean-field and QMD calculations.

However, if one includes the analysis of subthreshold kaon production [79, 80], all observables, which have been so far identified as sensitive to the nuclear EoS, point towards a soft momentum dependent EoS, maybe with a compressibility modulus slightly higher than that used presently for a soft equation-of-state. For neutron star physics, where the momentum dependence of the nucleon-nucleon potential is much less important, heavy-ion collisions delivers the message that the equation-of-state of cold symmetric matter for densities below $3\rho_0$ is soft with a compressibility modulus slightly higher than that used for a soft equation-of-state.

ACKNOWLEDGEMENTS

The authors acknowledge inspiring discussions with M. Bleicher, W. Cassing, H. Elfner, I. Grishmanovskii, C.-M. Ko, T. Reichert, N. Xu, O. Soloveva, T. Song, Io. Vassiliev. We acknowledge fruitful discussions with B. Kardan and his help for understanding of the HADES experimental data and acceptance. We thank M. Cassing for making an artistic plot in Fig. 29. Furthermore, we acknowledge support by the Deutsche Forschungsgemeinschaft (DFG, German Research Foundation) grant BL982-3, by the Russian Science Foundation grant 19-42-04101 and by the GSI-IN2P3 agreement under contract number 13-70. This study is part of a project that has received funding from the European Union's Horizon 2020 research and innovation program under grant agreement STRONG – 2020 - No 824093. The computational resources have been provided by the Center for Scientific Computing (CSC) of the Goethe University and the NICA LHEP offline cluster of the Joint Institute for Nuclear Research. V.K. thanks the Veksler and Baldin Laboratory of High Energy Physics for the support in the form of a scholarship named after academician Markov.

Appendix A: Momentum-dependent interaction in BUU versus QMD type models

In this Appendix we recall the conceptual differences in the realization of momentum-dependent potentials in QMD and BUU type approaches, which are essential for the interpretation of the experimental flow data. This has the consequence that, even if the same momentum-dependent potential is applied in QMD and BUU models, the final results for the observables might differ which complicates the determination of the EoS. This is due to the following reasons:

- as discussed in Section II A-C, the QMD equations-of-motion describe the propagation of single-particle wave functions in terms of Gaussian Wigner densities. There the two-body momentum-dependent potential $V(\mathbf{p}_{0i}, \mathbf{p}_{0j})$ depends on the momenta of each pair of interacting particles i, j - cf. Eq. (3), defined in the A+A "computational" frame (which is usually taken as the initial nucleon-nucleon center-of-mass frame).
- the BUU equations describe the propagation of a single-particle phase-space distribution of nucleons, employing a one-body (mean-field) Hamiltonian. The potential interaction is realized by density-dependent and momentum-dependent potentials. The latter is a function of the momentum of the considered particle with respect to the local cell at rest. We note that the BUU equations can be cast into a relativistic form contrary to the QMD equations, where the time evolution of the parameters is given by a variational principle based on the n -body Schrödinger equation.

The BUU equations are solved with a finite time-step method (employed also in the PHQMD/PHSD) using the

test-particle method, where one "physical" (initial) nucleon is presented by a swarm of N point-like test particles. This can be realized either via the parallel ensemble algorithm as in the PHSD (where test particles can collide only with others from their own ensemble and a communication between ensembles only occurs via mean-field quantities - density and energy density) or in the combined ensemble method as in SMASH (where all test particles are combined in one ensemble and nucleon-nucleon cross sections are scaled by $1/N$).

In the BUU the mean-field quantities - baryon, scalar and energy densities - are computed on grid cells in coordinate space. The forces, acting on test particles, are then a function of the density gradient of neighboring grid cells. For a sufficient number of test particles per nucleon this gives very stable results. As far as single particle observables are concerned, the QMD and BUU equations lead to very similar results - as tested in the PHQMD/PHSD framework.

However, the collective observables - such as flow coefficients - are more sensitive to the different treatment of the momentum-dependent interaction, since the flow starts to develop when the nuclei touch each other and where the relative momentum between target and projectile nucleons is large.

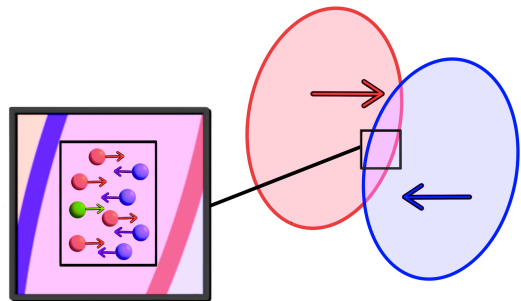


FIG. 29. Schematic presentation of the particle motion in the central cell of heavy-ion collision during the initial stage.

As an example, let's consider a cell in the nuclear overlap zone at the beginning of a A+A collision, when the nuclei just touch each other. This is schematically illustrated in Fig. 29. Since the initial nucleons from the target (violet dots) and the projectile (red dots) are moving with approximately the same magnitude of the velocity, but in opposite direction (let's neglect the Fermi motion for simplicity), the matter in the cell is practically stopped, i.e. the average velocity in the cell is close to zero. Assume that a nucleon, let's call it "test" nucleon (green dot), enters such cell with momentum \mathbf{p}_i in the calculational frame, which is practically identical to its momentum in center-of-mass frame of the cell, since the cell velocity is close to zero in our example. The key point is that the forces acting on this "test" nucleon are different in BUU and in QMD.

Indeed, in BUU the momentum dependent force is cal-

culated relative to the matter at rest, i.e. in the center-of-mass frame of the cell, and is thus (for nonrelativistic kinematics) proportional to

$$F^{BUU} = F(\mathbf{p}_i - \langle \mathbf{p}^{cell} \rangle) \approx F(\mathbf{p}_i).$$

because $\langle \mathbf{p}^{cell} \rangle$ is zero in the example above.

In QMD the forces depend on the relative momentum between two interacting nucleons $F^{QMD} = \langle \sum F(\mathbf{p}_i - \mathbf{p}_j) \rangle$. Since in the considered cell about 50% of nucleons are moving towards to the "test" nucleon, their momenta are orthogonal and approximately equal, such that the force acting on the "test" nucleon is proportional to $F_1^{QMD} = \langle F(\mathbf{p}_i - \mathbf{p}_j) \rangle \simeq \langle F(\mathbf{p}_i + \mathbf{p}_i) \rangle \simeq \langle F(2\mathbf{p}_i) \rangle$. The other 50 % of nucleons are comoving with the "test" nucleon with approximately the same parallel momentum. Therefore, the force acting on them is $F_2^{QMD} = \langle F(\mathbf{p}_i - \mathbf{p}_j) \rangle \simeq F(0)$ and hence is equal zero for the momentum-dependent potential considered in Fig. 1. The total force acting on the "test" nucleon in QMD is

then

$$F^{QMD} = \frac{1}{2}(\langle F^{QMD}(0) \rangle + \langle F^{QMD}(2\mathbf{p}_i) \rangle) \approx \frac{1}{2}\langle F(2\mathbf{p}_i) \rangle.$$

Consequently, only if the form of the momentum-dependent potential is such that $F(\mathbf{p}_i) \simeq \frac{1}{2}F(2\mathbf{p}_i)$, the forces in BUU and QMD are identical. For the realistic optical potential of the form of Fig. 1 this is not the case. For a non-central cell the situation is more complex. Whether the momentum-dependent potential gives initially more repulsion in BUU or QMD depends on the beam energy.

Due to this different realization of the momentum-dependent interaction in QMD and BUU type transport approaches, like the SMASH model [27], we do not expect exactly the same results for the flow coefficients v_1 and v_2 in heavy-ion collisions, even if in cold nuclear matter or for p-A collisions in the target rest frame the momentum-dependent interaction gives identical forces in both approaches.

-
- [1] H. A. Gustafsson *et al.*, Collective Flow Observed in Relativistic Nuclear Collisions, *Phys. Rev. Lett.* **52**, 1590 (1984).
- [2] H. Koehn *et al.*, An overview of existing and new nuclear and astrophysical constraints on the equation of state of neutron-rich dense matter, (2024), arXiv:2402.04172 [astro-ph.HE].
- [3] F. Ozel, D. Psaltis, S. Ransom, P. Demorest, and M. Alford, The Massive Pulsar PSR J1614-2230: Linking Quantum Chromodynamics, Gamma-ray Bursts, and Gravitational Wave Astronomy, *Astrophys. J. Lett.* **724**, L199 (2010), arXiv:1010.5790 [astro-ph.HE].
- [4] R. Lastowiecki, D. Blaschke, H. Grigorian, and S. Typel, Strangeness in the cores of neutron stars, *Acta Phys. Polon. Supp.* **5**, 535 (2012), arXiv:1112.6430 [nucl-th].
- [5] S. Bogdanov *et al.*, Constraining the Neutron Star Mass-Radius Relation and Dense Matter Equation of State with NICER. III. Model Description and Verification of Parameter Estimation Codes, *Astrophys. J. Lett.* **914**, L15 (2021), arXiv:2104.06928 [astro-ph.HE].
- [6] A. Bauswein, H. T. Janka, K. Hebeler, and A. Schwenk, Equation-of-state dependence of the gravitational-wave signal from the ring-down phase of neutron-star mergers, *Phys. Rev. D* **86**, 063001 (2012), arXiv:1204.1888 [astro-ph.SR].
- [7] E. R. Most, A. Motornenko, J. Steinheimer, V. Dexheimer, M. Hanauske, L. Rezzolla, and H. Stoecker, Probing neutron-star matter in the lab: Similarities and differences between binary mergers and heavy-ion collisions, *Phys. Rev. D* **107**, 043034 (2023), arXiv:2201.13150 [nucl-th].
- [8] W. Botermans and R. Malfliet, Quantum transport theory of nuclear matter, *Phys. Rept.* **198**, 115 (1990).
- [9] C. Fuchs, T. Wainzoch, A. Faessler, and D. S. Kosov, Scalar and vector decomposition of the nucleon self-energy in the relativistic Brueckner approach, *Phys. Rev. C* **58**, 2022 (1998).
- [10] C. Gale, G. Bertsch, and S. Das Gupta, Heavy-ion collision theory with momentum-dependent interactions, *Phys. Rev. C* **35**, 1666 (1987).
- [11] J. Aichelin, A. Rosenhauer, G. Peilert, H. Stoecker, and W. Greiner, Importance of Momentum Dependent Interactions for the Extraction of the Nuclear Equation of State From High-energy Heavy Ion Collisions, *Phys. Rev. Lett.* **58**, 1926 (1987).
- [12] C. M. Ko, Q. Li, and R.-C. Wang, Relativistic Vlasov Equation for Heavy Ion Collisions, *Phys. Rev. Lett.* **59**, 1084 (1987).
- [13] J. Aichelin, 'Quantum' molecular dynamics: A Dynamical microscopic n body approach to investigate fragment formation and the nuclear equation of state in heavy ion collisions, *Phys. Rept.* **202**, 233 (1991).
- [14] K. Weber, B. Blaettel, W. Cassing, H. C. Doenges, A. Lang, T. Maruyama, and U. Mosel, Relativistic potentials for a counterstreaming nuclear matter scenario with a covariant momentum dependent interaction, *Nucl. Phys. A* **552**, 571 (1993).
- [15] P. K. Sahu, A. Hombach, W. Cassing, and U. Mosel, Baryon flow at SIS energies and beyond, *Nucl. Phys. A* **640**, 493 (1998), arXiv:nucl-th/9801043.
- [16] P. Danielewicz, R. A. Lacey, P. B. Gossiaux, C. Pinkenburg, P. Chung, J. M. Alexander, and R. L. McGrath, Disappearance of elliptic flow: a new probe for the nuclear equation of state, *Phys. Rev. Lett.* **81**, 2438 (1998), arXiv:nucl-th/9803047.
- [17] P. K. Sahu, W. Cassing, U. Mosel, and A. Ohnishi, Baryon flow from SIS to AGS energies, *Nucl. Phys. A* **672**, 376 (2000), arXiv:nucl-th/9907002.
- [18] W. Cassing, E. L. Bratkovskaya, and S. Juchem, Excitation functions of hadronic observables from SIS to RHIC energies, *Nucl. Phys. A* **674**, 249 (2000), arXiv:nucl-th/0001024.
- [19] P. K. Sahu and W. Cassing, Differential flow of protons in Au+Au collisions at AGS energies, *Nucl. Phys. A* **712**,

- 357 (2002), arXiv:nucl-th/0208002.
- [20] Y. Nara, T. Maruyama, and H. Stoecker, Momentum-dependent potential and collective flows within the relativistic quantum molecular dynamics approach based on relativistic mean-field theory, *Phys. Rev. C* **102**, 024913 (2020), arXiv:2004.05550 [nucl-th].
- [21] J. J. Molitoris, D. Hahn, and H. Stoecker, Circumstantial Evidence for a Stiff Nuclear Equation of State, *Nucl. Phys. A* **447**, 13C (1986).
- [22] E. D. Cooper, S. Hama, and B. C. Clark, Global Dirac optical potential from helium to lead, *Phys. Rev. C* **80**, 034605 (2009).
- [23] M. Bleicher and E. Bratkovskaya, Modelling relativistic heavy-ion collisions with dynamical transport approaches, *Prog. Part. Nucl. Phys.* **122**, 103920 (2022).
- [24] H. Wolter *et al.* (TMEP), Transport model comparison studies of intermediate-energy heavy-ion collisions, *Prog. Part. Nucl. Phys.* **125**, 103962 (2022), arXiv:2202.06672 [nucl-th].
- [25] A. Sorensen *et al.*, Dense nuclear matter equation of state from heavy-ion collisions, *Prog. Part. Nucl. Phys.* **134**, 104080 (2024), arXiv:2301.13253 [nucl-th].
- [26] P. Hillmann, J. Steinheimer, T. Reichert, V. Gaebel, M. Bleicher, S. Sombun, C. Herold, and A. Limphirat, First, second, third and fourth flow harmonics of deuterons and protons in Au+Au reactions at 1.23 AGeV, *J. Phys. G* **47**, 055101 (2020), arXiv:1907.04571 [nucl-th].
- [27] L. A. Tarasovičová, J. Mohs, A. Andronic, H. Elfner, and K.-H. Kampert, Flow and Equation of State of nuclear matter at $E_{\text{kin}}/A=0.25\text{-}1.5$ GeV with the SMASH transport approach, (2024), arXiv:2405.09889 [nucl-th].
- [28] W. Reisdorf *et al.* (FOPI), Systematics of central heavy ion collisions in the 1A GeV regime, *Nucl. Phys. A* **848**, 366 (2010), arXiv:1005.3418 [nucl-ex].
- [29] T. Anticic *et al.* (NA49), Energy and centrality dependence of deuteron and proton production in Pb + Pb collisions at relativistic energies, *Phys. Rev. C* **69**, 024902 (2004).
- [30] T. Anticic *et al.* (NA49), Production of deuterium, tritium, and He3 in central Pb + Pb collisions at 20A,30A,40A,80A , and 158A GeV at the CERN Super Proton Synchrotron, *Phys. Rev. C* **94**, 044906 (2016), arXiv:1606.04234 [nucl-ex].
- [31] J. Adam *et al.* (STAR), Beam energy dependence of (anti-)deuteron production in Au + Au collisions at the BNL Relativistic Heavy Ion Collider, *Phys. Rev. C* **99**, 064905 (2019), arXiv:1903.11778 [nucl-ex].
- [32] J. Adam *et al.* (ALICE), Production of light nuclei and anti-nuclei in pp and Pb-Pb collisions at energies available at the CERN Large Hadron Collider, *Phys. Rev. C* **93**, 024917 (2016), arXiv:1506.08951 [nucl-ex].
- [33] J. Adam *et al.* (STAR), Beam energy dependence of (anti-)deuteron production in Au + Au collisions at the BNL Relativistic Heavy Ion Collider, *Phys. Rev. C* **99**, 064905 (2019), arXiv:1903.11778 [nucl-ex].
- [34] M. Abdulhamid *et al.* (STAR), Beam Energy Dependence of Triton Production and Yield Ratio ($N_t \times N_p / N_d^2$) in Au+Au Collisions at RHIC, *Phys. Rev. Lett.* **130**, 202301 (2023), arXiv:2209.08058 [nucl-ex].
- [35] A. Andronic, P. Braun-Munzinger, J. Stachel, and H. Stoecker, Production of light nuclei, hypernuclei and their antiparticles in relativistic nuclear collisions, *Phys. Lett. B* **697**, 203 (2011), arXiv:1010.2995 [nucl-th].
- [36] S. T. Butler and C. A. Pearson, Deuterons from High-Energy Proton Bombardment of Matter, *Phys. Rev.* **129**, 836 (1963).
- [37] L. Zhu, C. M. Ko, and X. Yin, Light (anti-)nuclei production and flow in relativistic heavy-ion collisions, *Phys. Rev. C* **92**, 064911 (2015), arXiv:1510.03568 [nucl-th].
- [38] W. Zhao, C. Shen, C. M. Ko, Q. Liu, and H. Song, Beam-energy dependence of the production of light nuclei in Au + Au collisions, *Phys. Rev. C* **102**, 044912 (2020), arXiv:2009.06959 [nucl-th].
- [39] K.-J. Sun, R. Wang, C. M. Ko, Y.-G. Ma, and C. Shen, Relativistic kinetic approach to light nuclei production in high-energy nuclear collisions, (2021), arXiv:2106.12742 [nucl-th].
- [40] S. Sombun, K. Tomuang, A. Limphirat, P. Hillmann, C. Herold, J. Steinheimer, Y. Yan, and M. Bleicher, Deuteron production from phase-space coalescence in the UrQMD approach, *Phys. Rev. C* **99**, 014901 (2019), arXiv:1805.11509 [nucl-th].
- [41] V. Kireyeu, J. Steinheimer, J. Aichelin, M. Bleicher, and E. Bratkovskaya, Deuteron production in ultrarelativistic heavy-ion collisions: A comparison of the coalescence and the minimum spanning tree procedure, *Phys. Rev. C* **105**, 044909 (2022), arXiv:2201.13374 [nucl-th].
- [42] J. Aichelin, E. Bratkovskaya, A. Le Fèvre, V. Kireyeu, V. Kolesnikov, Y. Leifels, V. Voronyuk, and G. Coci, Parton-hadron-quantum-molecular dynamics: A novel microscopic n -body transport approach for heavy-ion collisions, dynamical cluster formation, and hypernuclei production, *Phys. Rev. C* **101**, 044905 (2020), arXiv:1907.03860 [nucl-th].
- [43] S. Gläsel, V. Kireyeu, V. Voronyuk, J. Aichelin, C. Blume, E. Bratkovskaya, G. Coci, V. Kolesnikov, and M. Winn, Cluster and hypercluster production in relativistic heavy-ion collisions within the parton-hadron-quantum-molecular-dynamics approach, *Phys. Rev. C* **105**, 014908 (2022), arXiv:2106.14839 [nucl-th].
- [44] G. Coci, S. Gläsel, V. Kireyeu, J. Aichelin, C. Blume, E. Bratkovskaya, V. Kolesnikov, and V. Voronyuk, Dynamical mechanisms for deuteron production at mid-rapidity in relativistic heavy-ion collisions from energies available at the GSI Schwerionensynchrotron to those at the BNL Relativistic Heavy Ion Collider, *Phys. Rev. C* **108**, 014902 (2023), arXiv:2303.02279 [nucl-th].
- [45] D. Oliinychenko, C. Shen, and V. Koch, Deuteron production in AuAu collisions at $\sqrt{s_{NN}}=7\text{-}200$ GeV via pion catalysis, *Phys. Rev. C* **103**, 034913 (2021), arXiv:2009.01915 [hep-ph].
- [46] J. Staudenmaier, D. Oliinychenko, J. M. Torres-Rincon, and H. Elfner, Deuteron production in relativistic heavy ion collisions via stochastic multiparticle reactions, *Phys. Rev. C* **104**, 034908 (2021), arXiv:2106.14287 [hep-ph].
- [47] V. Kireyeu, G. Coci, S. Gläsel, J. Aichelin, C. Blume, and E. Bratkovskaya, Cluster formation near midrapidity: How the production mechanisms can be identified experimentally, *Phys. Rev. C* **109**, 044906 (2024).
- [48] J. Adamczewski-Musch *et al.* (HADES), Directed, Elliptic, and Higher Order Flow Harmonics of Protons, Deuterons, and Tritons in Au + Au Collisions at $\sqrt{s_{NN}} = 2.4$ GeV, *Phys. Rev. Lett.* **125**, 262301 (2020), arXiv:2005.12217 [nucl-ex].
- [49] J. Adamczewski-Musch *et al.* (HADES), Proton, deuteron and triton flow measurements in Au+Au collisions at $\sqrt{s_{NN}} = 2.4$ GeV, *Eur. Phys. J. A* **59**, 80 (2023), arXiv:2208.02740 [nucl-ex].

- [50] W. Reisdorf *et al.* (FOPI), Systematics of azimuthal asymmetries in heavy ion collisions in the 1 A GeV regime, *Nucl. Phys. A* **876**, 1 (2012), arXiv:1112.3180 [nucl-ex].
- [51] J. Steinheimer, T. Reichert, Y. Nara, and M. Bleicher, Momentum dependent potentials from a parity doubling CMF model in UrQMD: Results on flow and particle production, (2024), arXiv:2410.01742 [hep-ph].
- [52] J. Aichelin, A. Bohnet, G. Peilert, H. Stoecker, W. Greiner, and A. Rosenhauer, Quantum Molecular Dynamics Approach to Heavy Ion Collisions: Description of the Model, Comparison With Fragmentation Data, and the Mechanism of Fragment Formation, *Phys. Rev. C* **37**, 2451 (1988).
- [53] C. Hartnack, R. K. Puri, J. Aichelin, J. Konopka, S. A. Bass, H. Stoecker, and W. Greiner, Modeling the many body dynamics of heavy ion collisions: Present status and future perspective, *Eur. Phys. J. A* **1**, 151 (1998), arXiv:nucl-th/9811015.
- [54] W. Cassing and E. L. Bratkovskaya, Parton transport and hadronization from the dynamical quasiparticle point of view, *Phys. Rev. C* **78**, 034919 (2008), arXiv:0808.0022 [hep-ph].
- [55] W. Cassing, From Kadanoff-Baym dynamics to off-shell parton transport, *Eur. Phys. J. ST* **168**, 3 (2009), arXiv:0808.0715 [nucl-th].
- [56] W. Cassing and E. L. Bratkovskaya, Parton-Hadron-String Dynamics: an off-shell transport approach for relativistic energies, *Nucl. Phys. A* **831**, 215 (2009), arXiv:0907.5331 [nucl-th].
- [57] E. L. Bratkovskaya, W. Cassing, V. P. Konchakovski, and O. Linnyk, Parton-Hadron-String Dynamics at Relativistic Collider Energies, *Nucl. Phys. A* **856**, 162 (2011), arXiv:1101.5793 [nucl-th].
- [58] O. Linnyk, E. L. Bratkovskaya, and W. Cassing, Effective QCD and transport description of dilepton and photon production in heavy-ion collisions and elementary processes, *Prog. Part. Nucl. Phys.* **87**, 50 (2016), arXiv:1512.08126 [nucl-th].
- [59] P. Moreau, O. Soloveva, L. Oliva, T. Song, W. Cassing, and E. Bratkovskaya, Exploring the partonic phase at finite chemical potential within an extended off-shell transport approach, *Phys. Rev. C* **100**, 014911 (2019), arXiv:1903.10257 [nucl-th].
- [60] B. C. Clark, E. D. Cooper, and S. Hama, Global Dirac phenomenology for proton elastic scattering from He4, *Phys. Rev. C* **73**, 024608 (2006).
- [61] E. D. Cooper, S. Hama, B. C. Clark, and R. L. Mercer, Global Dirac phenomenology for proton nucleus elastic scattering, *Phys. Rev. C* **47**, 297 (1993).
- [62] M. Jaminon, C. Mahaux, and P. Rochus, OPTICAL MODEL POTENTIAL IN A RELATIVISTIC QUANTUM FIELD MODEL, *Phys. Rev. C* **22**, 2027 (1980).
- [63] A. Le Fèvre, Y. Leifels, C. Hartnack, and J. Aichelin, Origin of elliptic flow and its dependence on the equation of state in heavy ion reactions at intermediate energies, *Phys. Rev. C* **98**, 034901 (2018), arXiv:1611.07500 [nucl-th].
- [64] O. Buss, T. Gaitanos, K. Gallmeister, H. van Hees, M. Kaskulov, O. Lalakulich, A. B. Larionov, T. Leitner, J. Weil, and U. Mosel, Transport-theoretical Description of Nuclear Reactions, *Phys. Rept.* **512**, 1 (2012), arXiv:1106.1344 [hep-ph].
- [65] J. Mohs, M. Ege, H. Elfner, and M. Mayer (SMASH), Collective flow at SIS energies within a hadronic transport approach: Influence of light nuclei formation and equation of state, *Phys. Rev. C* **105**, 034906 (2022), arXiv:2012.11454 [nucl-th].
- [66] A. Raab, *Chem. Phys. Lett.* **319**, 674 (2000).
- [67] J. Broeckhove, L. Lathouwers, E. Kesteloot, and P. Van Leuven, On the equivalence of time-dependent variational principles, *Chemical Physics Letters* **149**, 547 (1988).
- [68] H. Feldmeier, FERMIONIC MOLECULAR DYNAMICS, *Nucl. Phys. A* **515**, 147 (1990).
- [69] A. Ono, H. Horiuchi, T. Maruyama, and A. Ohnishi, Antisymmetrized version of molecular dynamics with two nucleon collisions and its application to heavy ion reactions, *Prog. Theor. Phys.* **87**, 1185 (1992).
- [70] J.-Y. Ollitrault, On the measurement of azimuthal anisotropies in nucleus-nucleus collisions, (1997), arXiv:nucl-ex/9711003.
- [71] A. M. Poskanzer and S. A. Voloshin, Methods for analyzing anisotropic flow in relativistic nuclear collisions, *Phys. Rev. C* **58**, 1671 (1998), arXiv:nucl-ex/9805001.
- [72] B. Towseef, M. Farooq, V. Bairathi, B. Waseem, S. Kabana, and S. Ahmad, Elliptic flow of identified hadrons in Au+Au collisions at $E_{lab} = 35$ A GeV using the PHSD model, *Eur. Phys. J. C* **83**, 649 (2023), [Erratum: *Eur. Phys. J. C* **83**, 682 (2023)], arXiv:2302.11772 [nucl-ex].
- [73] A. Z. Mekjian and L. Zamick, Nuclear equation of state and incompressibility in a model with correlations from giant monopole vibrations, *Phys. Rev. C* **85**, 044318 (2012), arXiv:1112.0457 [nucl-th].
- [74] T. Reichert and J. Aichelin, to be published.
- [75] B. Kardan, private communications.
- [76] R. J. Fries, B. Muller, C. Nonaka, and S. A. Bass, Hadron production in heavy ion collisions: Fragmentation and recombination from a dense parton phase, *Phys. Rev. C* **68**, 044902 (2003), arXiv:nucl-th/0306027.
- [77] J. Adams *et al.* (STAR), Particle type dependence of azimuthal anisotropy and nuclear modification of particle production in Au + Au collisions at $s(\text{NN})^{1/2} = 200$ -GeV, *Phys. Rev. Lett.* **92**, 052302 (2004), arXiv:nucl-ex/0306007.
- [78] A. Adare *et al.* (PHENIX), Scaling properties of azimuthal anisotropy in Au+Au and Cu+Cu collisions at $s(\text{NN}) = 200$ -GeV, *Phys. Rev. Lett.* **98**, 162301 (2007), arXiv:nucl-ex/0608033.
- [79] C. Hartnack, H. Oeschler, and J. Aichelin, Hadronic matter is soft, *Phys. Rev. Lett.* **96**, 012302 (2006), arXiv:nucl-th/0506087.
- [80] C. Hartnack, H. Oeschler, Y. Leifels, E. L. Bratkovskaya, and J. Aichelin, Strangeness Production close to Threshold in Proton-Nucleus and Heavy-Ion Collisions, *Phys. Rept.* **510**, 119 (2012), arXiv:1106.2083 [nucl-th].